Numerical verification of the exact WKB formula for the generalized Landau-Zener-Stueckelberg problem

Naoaki Shimada and Akira Shudo
Department of Physics, Tokyo Metropolitan University, Minami-Osawa, Hachioji 192-0397, Japan

(Received 22 May 2020; accepted 15 July 2020; published 17 August 2020)

The WKB analysis for higher order differential equations had not been developed until recent progress of the so-called exact WKB method, so it was difficult to find WKB solutions for multistate nonadiabatic models in general, whereas enormous efforts were made especially for the study of generalized Landau-Zener models. Under such circumstances Aoki-Kawai-Takei provided a closed expression for the S matrix of a time-dependent multistate nonadiabatic system, in which diabatic potential curves are given as polynomial functions of time and they all intersect with each other. Their result is completely explicit, and the model covers much wider classes of systems than multistate nonadiabatic models studied so far. Here we numerically show how their exact WKB formula works as long as crossing points of diabatic potential curves are well separated. The model studied includes the cases where diabatic potential functions are nonlinear, not like generalized Landau-Zener models. We also discuss the situations where virtual turning points and new Stokes curves, new components in the Stokes geometry appearing only for higher order differential equations, come into play. In particular, we examine how the presence of new Stokes curves affects final transition probabilities using a couple of concrete examples.

DOI: 10.1103/PhysRevA.102.022213

I. INTRODUCTION

Nonadiabatic transitions are ubiquitous phenomena in dynamics of complex quantum systems. In molecules or atoms, dynamics of electrons are fast enough as compared with that of nuclei, the motions are almost decoupled with each other. As a result we may consider the dynamics of electrons at each time with the position of nuclei begin fixed. This is a situation referred to as the adiabatic limit, and the so-called Born-Oppenheimer approximation could be applied.

In actual situations, however, the ratio between the mass of electrons and nuclei is small but finite, so there happens the transition between the adiabatic states and such a transition is called the *nonadiabatic transition* [1]. It appears not only in atomic and molecular dynamics but also in dynamics taking place in solid and condensed matters.

A reasonable approach to describe the nonadiabatic transition, which in general expected to proceed among many states interacting with each other, is to reduce the problem to a two-state model. In particular, the simplest and most broadly established model is the Landau-Zener (LZ) model [2,3]:

$$i\hbar\frac{d}{dt}\psi = H(t)\psi, \tag{1}$$

where

$$H(t) = \begin{pmatrix} \alpha_1 t & c_{12} \\ c_{12} & \alpha_2 t \end{pmatrix} \tag{2}$$

and $\psi = {}^t(\psi_1, \psi_2)$. Here α_1, α_2, and c_{12} are constants not depending on time t. The probability of remaining at the initial state was evaluated by Landau [2], Zener [3], Mayorana [4], and Stueckelberg [5] in various ways, ranging from obtaining the exact solution to applying approximations including the WKB (Wentzel-Kramers-Brillouin) method [6–8]. The LZ model is simple in that it describes nonadiabatic transitions only between two states, and the diabatic energy levels depend on time t linearly.

It would be natural to extend such a simple two-state model to more general ones by increasing the number of states and/or by modifying the time dependence of matrix elements. The most well studied models are the cases in which the number of states is increased to more than two, keeping the linear dependence on time. Such multistate models are often called the generalized multistate Landau-Zener model (MLZ). The original LZ model can be reduced to the Weber equation, for which a solution in an integral representation is known, but it is hard in general to analytically solve the MLZ model. We can easily see the difficulty of finding solutions because, if one reduces a coupled equations for multistate models to a single equation, the degree of the equation becomes more than two, thereby one has to cope with higher order differential equations, for which much less is known in finding their solutions compared to the second order ones.

Enormous efforts have been made, nevertheless, to obtain solutions of multistate models and numerous results have been reported, especially for the MLZ model. The model, in which a single tiled diabatic energy crosses a set of several parallel energies, was first solved by applying the contour integral method [9,10], and it was extended to a class of multiple crossing grid models, in which rectilinear parallel diabatic energies cross each other, including a more generalized version [11–23]. Recent remarkable progress is a finding of the integrability condition which enables us to seek new solvable models [18–23].

Another class of models extensively studied so far is the so-called bow-tie model, in which a finite number of diabatic levels cross simultaneously at a single point. The bow-tie model was first solved for the system with a special symmetry [24], and later for more general cases [25]. An analytic solution for the model with an arbitrary number of states was presented in Ref. [26], and further generalization was made by introducing an additional parameter in order to investigate a specific signature of interaction of the model [27], and its exact solution was then given [28].

Analytical studies for multistate nonadiabatic transition models were performed not only for the models whose diabatic levels depend linearly on time, but for a class of the system in which one of the diabatic potential curves has Coulombic time dependence, whereas the rest of the diabatic levels are flat [15,29–31].

Solvability of MLZ models depends crucially on whether one can apply the *independent crossing approximation* [32]. At each crossing point of diabatic states, the multistate system is supposed to be reduced to the two-state system, so one may essentially apply the LZ formula there if one is allowed to ignore the interference between each state, or alternatively, dynamical phases accumulated in the course of time [18–20,22,23,26,27,33,34]. In the cases where the independent crossing approximation can be applied, the whole transition probability from $t = -\infty$ to $+\infty$ is expressed simply as a multiplication of LZ probabilities. To incorporate the dynamical phase between transitions at each crossing point properly, a recipe was proposed in which matrices, whose phases are given by integrating the adiabatic energy, should be multiplied in between the LZ matrices [35,36].

The analysis to ensure the validity of the independent crossing approximation is mainly based on the semiclassical ansatz. The path interference assumes multiple semiclassical waves propagating with time and the relative phases associated with each wave determines solvability of the model. The semiclassical theory would be helpful not only to gain an intuitive picture for what happens in the whole process, but to find purely rigorous solutions.

In this article we will examine the WKB formula for a multistate nonadiabatic transition model, which was derived by Aoki-Kawai-Takei [37]. Their analysis is based on the so-called *exact WKB method*, sometimes referred to as resurgent theory, or exponential asymptotics, depending on the context. The model studied there contains not only the MLZ model but also much wider classes of systems including the situations where diabatic potential terms are given as nonlinear functions of time. They gave a closed and explicit expression of the S matrix for the MLZ model and a concrete recipe to derive it in more general cases.

As is well known, the WKB method has been broadly used to obtain asymptotic solutions of ordinary (and partial) differential equations with a small (or large) parameter. However, WKB solutions are asymptotic at most and divergent in general, thereby ambiguities remain in its actual treatment. In particular, controlling the exponentially small terms is usually beyond the treatment of asymptotic expansions, so the Stokes phenomenon, discontinuous switching of WKB solutions in a parameter space, could have been argued only in a heuristic manner. This also made it difficult to apply the WKB method to higher order differential equations.

The exact WKB method has overcome such a difficulty inevitable in the divergent expansion through the Borel resummation method and provided an analytical basis for asymptotic expansions [38–44]. As a fruitful outcome, we are able to treat exponentially small terms in a proper manner, allowing us to attack the problems that would be out of reach of the conventional WKB argument. Owing to the development of the exact WKB analysis, we now know how the WKB method should be applied to higher order differential equations.

The most important ingredients treating the Stokes phenomenon are turning points and Stokes curves. It is easy to show that Stokes curves for second order differential equations never cross, whereas Stokes curves for higher order differential equations happen to cross. This was first pointed out explicitly by Berk, Nevins, and Roberts in their analysis of a certain third order ordinary differential equation [45]. They developed an argument, within a conventional WKB approach, that if one applies the standard connection formula around a crossing point of Stokes curves, the results depend on the connection pathway one takes. To dissolve such a puzzling situation, they proposed that *new Stokes curves* should be introduced. Their argument was entirely reasonable, but it was rather phenomenological and generalizability to other situations was not clear enough.

The work by Aoki, Kawai, and Takei was the first attempt to investigate Stokes phenomena in higher order differential equations within the exact WKB framework [46,47] (see also [48–50]). (A comprehensive review on this subject was found in Ref. [51].) They first studied a similar class of third order differential equations, including the one studied in Ref. [45], and gave a theorem, under suitable conditions, guaranteeing that the operation of local connection formulas established in second order cases holds as well. This means that local aspects of the exact WKB treatment are not affected even if one considers higher order cases [46]. More importantly, concerning the global property, they claimed that basic objects are not new Stokes curves but *virtual turning points* ("new turning points" was used in the first paper [46]), and *new Stokes curves*, emanating from a virtual turning point, are essentially the same as the Stokes curves known already.

It was, therefore, reasonable to employ such newly developed machinery for analyzing multistate nonadiabatic models, and it was indeed done in Ref. [37]. Under these circumstances, the objective of our paper is first to numerically verify how the WKB formula thus derived works in describing the multistate nonadiabatic transition. We especially take and test the leading order expression although they have provided a systematic recipe to obtain higher order terms with respect to the Planck constant because the leading order formula gives an intuitive picture for the whole process and might also be helpful for finding optimal control protocols for quantum dynamics. When truncating at the leading order, as is usually done in the WKB calculation, one might take into account uniform approximations if turning points are nearly coalesced with each other, so checking the validity and limitation for the leading order formula will be important as well.

It would be of particular importance to check whether the formula works even in *nonintegrable* MLZ models because

the WKB formula derived in [37] holds for generic MLZ models, and at the same time, it must be helpful for arguments on solvability of MLZ models. Furthermore, as a recipe to find an explicit S matrix was given not only for MLZ models but also for the models in which diabatic potential terms are given as polynomial functions of time. As mentioned above, known solvable models with nonlinear diabatic potentials are limited, so it would be worth examining whether even nonlinear models could be handled within the recipe proposed there.

Our second motivation here is to study the situations where some of the turning points are located in the complex plane. As shown in Ref. [37], if all the turning points are real, we may ignore new ingredients, such as virtual turning points and new Stokes curves, and only need to take into account standard ingredients which appear even in the two-state model. On the other hand, new objects may come into play when some turning points fall into the complex plane. Hence it will become a crucial task to identify the role of virtual turning points and new Stokes curves, in order to identify many state effects. There are, before proceeding with the analysis, some technical issues which should be carefully treated in the exact WKB analysis. When complex turning points appear in the model, they are sometimes connected by a single Stokes curve, and it is known that such a situation is beyond the treatment of the exact WKB treatment [44]. Thus to see the effect of new objects we have to consider how to cope with the degeneracy of Stokes curves.

The organization of the paper is as follows. In Sec. II we will present the form of the WKB solution and the associated connection formula for the Stokes phenomenon. They are basically given in Refs. [37,51] even in a more comprehensive and rigorous manner. We here provide a brief sketch of the idea of the derivation in order that even the readers not familiar with the exact WKB analysis can access and utilize the formula. In Sec. III we numerically verify the validity of the leading order WKB approximation for the cases where all the diabatic solutions intersect and the resulting turning points for Stokes phenomena are all located on the real axis of the time plane. In this case, the S matrix can be given explicitly not only in the case where diabatic energy levels are linearly dependent on time, but also in the case where they depend on time in a nonlinear way. In Sec. IV we explore the role of virtual turning points and new Stokes curves, especially focusing on their observability taking a couple of models as examples in which those new objects are expected to contribute. In the Appendices we put brief derivations for some formulas employed in calculations. The exact WKB analysis or resurgent theory has been developed mainly by mathematicians, and it looks so formal that one could not apply it to the analysis of concrete models. Our motivation throughout the present paper is to show that this is not the case.

II. THE WKB FORMULA AND STOKES GEOMETRY

Hereafter we consider the following three-level nonadiabatic transition model

$$i\frac{d}{dt}\psi = \eta H(t,\eta)\psi, \tag{3}$$

where $\eta = 1/\hbar$ is a large parameter, and $\psi = {}^t(\psi_1, \psi_2, \psi_3)$ denotes a three vector. $H(t,\eta)$ takes the form as

$$H(t,\eta) = H_0(t) + \eta^{-1/2}H_{1/2}, \tag{4}$$

with a diagonal matrix depending on time t,

$$H_0(t) = \begin{pmatrix} \rho_1(t) & 0 & 0 \\ 0 & \rho_2(t) & 0 \\ 0 & 0 & \rho_3(t) \end{pmatrix}, \tag{5}$$

and an off-diagonal coupling is given by

$$H_{1/2} = \begin{pmatrix} 0 & c_{12} & c_{13} \\ \overline{c_{12}} & 0 & c_{23} \\ \overline{c_{13}} & \overline{c_{23}} & 0 \end{pmatrix}. \tag{6}$$

Here $\rho_j(t)$ $(j = 1, 2, 3)$ is assumed to a real polynomial and c_{ij} $(j, k = 1, 2, 3)$ are complex constants [37]. First we note that an extra factor $\eta^{-1/2}$ appears in front of the off-diagonal matrix, which is absent in ordinary nonadiabatic transition models. This factor is inserted just as a formal requirement which makes the Borel transform and the Borel sum of the WKB solution be readily defined [37]. The WKB solution for Eq. (3) will be given by assuming that η is a large parameter. In numerical calculations performed below, we often put $\eta = 1$ or adjust the magnitude of off-diagonal terms c_{ij} in a proper way. The form (3) is known as the diabatic representation of a nonadiabatic Hamiltonian. Since the off-diagonal term multiplied by $\eta^{-1/2}$ is regarded as a perturbation, the WKB approximation is expected to get better with an increase in η, that is, in the diabatic limit.

It should be noted that any polynomials are allowed in the diagonal term, so the model includes not only a class of MLZ models but also the ones with nonlinear diabatic energy levels. As a result, this model could cover much broader situations than MLZ models. In the paper [37] it was assumed that

$$[\rho_1(t) - \rho_2(t)]\,[\rho_2(t) - \rho_3(t)]\,[\rho_3(t) - \rho_1(t)] = 0$$
$$\text{has only real and simple zeros.} \tag{7}$$

This means that crossing points of diabatic energy levels are all real valued. Hereafter the condition (7) will be referred to as the *reality condition*. As argued in Sec. III, this greatly simplifies the problem and makes it possible to write down explicitly the S matrix [37]. In the present paper, in addition to such simple situations, we will investigate more general cases where the above condition is violated.

We briefly sketch a concrete recipe for calculating the S matrix for the system (3). Let $\psi^{(j)}$ $(j = 1, 2, 3)$ be a WKB solution for the system (3), and $\psi^{\pm,(j)} := N^{\pm,(j)}\psi^{(j)}$ a normalized solution determined in such a way that

$$\lim_{t\to\pm\infty} |\psi_k^{\pm,(j)}| = \delta_{jk} \quad (j, k = 1, 2, 3), \tag{8}$$

where $N^{\pm,(j)}$ $(j = 1, 2, 3)$ denote normalization constants introduced by taking into account the multivaluedness appearing in the WKB solution [37]. Then the S-matrix S is expressed as

$$S = N^{(+)}\widetilde{S}N^{(-)}, \tag{9}$$

where $N^{(+)}$ $(N^{(-)})$ is an appropriate normalization matrix for $t \to +\infty$ $(t \to -\infty)$, and $\widetilde{S}$ stands for the *connection matrix*,

which will be a major matter of concern in the following analysis. It is our final goal to obtain the S matrix for given diabatic energy levels $\rho_j(t)$ $(j = 1, 2, 3)$ and the off-diagonal constants c_{jk} $(j, k = 1, 2, 3)$. Before calculating the connection matrix $\widetilde{S}$ first we have to construct the WKB solutions and then prepare the connection formula due to Stokes phenomena between the WKB solutions. Below we briefly explain how each step can be achieved.

A. Construction of a WKB solution

Constructing the WKB solutions is actually made by transforming the original equation (3) for $\psi = {}^t(\psi_1, \psi_2, \psi_3)$ into a decoupled equation for $\varphi = {}^t(\varphi_1, \varphi_2, \varphi_3)$ [37]. Here a function φ is given by

$$\psi = R(t, \eta)\varphi,$$

with

$$R(t, \eta) = [1 + \eta^{-1/2}P_{1/2}(t)][1 + \eta^{-1}P_1(t)]\cdots,$$

where $P_{n/2}(t)$ $(n = 1, 2, \dots)$ are unknown functions, which are recursively defined in such a way that the equation for φ should take the form as

$$i\frac{d}{dt}\varphi = \eta[H_0(t) + \eta^{-1}\widetilde{H}_1(t) + \eta^{-3/2}\widetilde{H}_{3/2}(t) + \cdots]\varphi,$$

where each matrix $\widetilde{H}_{n/2}(t)$ becomes diagonal. This diagonal system admits a formal solution for Eq. (3),

$$\psi^{(j)} = \exp\Big(\frac{\eta}{i}\int_t \rho_j(t)dt\Big)\sum_{m=0}^{\infty}\psi^{(j)}_{m/2}(t)\eta^{-(m+1/2)}.$$

A more explicit expression is given as

$$\psi^{(j)} = \eta^{-1/2}\exp\Bigg[\frac{\eta}{i}\int^t \rho_j(t)dt + \frac{1}{i}\int^t\Big(\frac{|c_{jk}|^2}{\rho_j - \rho_k} + \frac{|c_{jl}|^2}{\rho_j - \rho_l}\Big)dt\Bigg]\big(e^{(j)} + O(\eta^{-1/2})\big), \tag{10}$$

where $e^{(j)}$ is a unit vector satisfying $e^{(\alpha)}_\beta = \delta_{\alpha\beta}$.

B. Derivation of the connection formula

The next step is to consider the connection of WKB solutions across a Stokes curve. As shown by Zener [3], the two-state model can be reduced to the Weber equation, so we expect that the same structure appears at least locally for the multistate model unless accidental degeneracy of turning points happens. This naive expectation frequently appears in preceding studies for multistate models and actually has been used as an ansatz to treat multistate models. However, as is shown in Refs. [37,51] and actually presented below, we need to construct proper WKB solutions with carefully chosen normalization. This is because the issue is entirely global in nature although one is apparently allowed to treat it locally as far as one focuses on the vicinity of a turning point. Below we present the connection formula for WKB solutions $\psi^{(j)}$ $(j = 1, 2, 3)$ derived in Refs. [37,51]. Some details necessary for actually applying the formula are provided in Appendix A, but more explicit calculations especially for generalized Landau-Zener model, in which the diagonal levels $\rho^{(j)}(t)$ $(j = 1, 2, 3)$ are given as linear functions of t, are found in Ref. [37].

We here restrict ourselves to the situation where the reality condition (7) holds. If the reality condition is satisfied, virtual turning points, a new type of turning points, and new Stokes curves will not actually contribute in constructing the S matrix or the connection matrix although those new ingredients appear even in such a situation. Therefore, at the moment until such new objects play a role, turning points and Stokes curves in the ordinary sense will only be considered. Hereafter, to distinguish new components they are specifically called *ordinary turning points* and *ordinary Stokes curves*, respectively. Note that ordinary turning points are located on the real t axis if the reality condition (7) holds.

More precisely, a point $t = \tau$ is said to be an ordinary turning point of type (j, k) if

$$\rho_j(\tau) = \rho_k(\tau) \tag{11}$$

for some j and k with $j \neq k$. The associated ordinary Stokes curves are given by the condition

$$\mathrm{Im}\Big[\frac{1}{i}\int_\tau^t(\rho_j(\tau) - \rho_k(\tau))dt\Big] = 0. \tag{12}$$

We put the name of *Stokes geometry* in order to represent the set of turning points, including virtual turning points introduced afterwards, and Stokes curves, including new Stokes curves. We will provide a more precise definition in Sec. IV B. The Stokes geometry is a purely topological object and can be identified as a graph consisting of vertices (turning points) and edges (Stokes curves) [52].

In the case of the multistate model satisfying the reality condition, ordinary turning points are aligned on the real t axis. Let $\{t^{[n]}_{j_n,k_n}\}_{n=1,\dots,N}$ be ordinary turning points arranged in an increasing order on the t axis, where $t^{[n]}_{j_n,k_n}$ is of the type (j_n, k_n). We further assume that

$$\lambda^{[n]}_{j_n,k_n} = \frac{d}{dt}(\rho_k(\tau) - \rho_j(\tau))\big|_{t^{[n]}_{j_n,k_n}} > 0 \tag{13}$$

for any n.

When $\psi^{(j)}$ $(j = 1, 2, 3)$ are analytically continued from the left to the right across the two Stokes curves emanating from a turning point $t^{[n]}_{j,k}$ in the upper half-plane, the connection formula for $\psi^{(j)}$ $(j = 1, 2, 3)$ can be expressed as

$$\begin{aligned}\psi^{(j)} &\longmapsto \big(1 + \alpha^{[n],-}_{jk}\alpha^{[n],+}_{jk}\big)\psi^{(j)} - \alpha^{[n],-}_{jk}\psi^{(k)},\\ \psi^{(k)} &\longmapsto \psi^{(k)} - \alpha^{[n],+}_{jk}\psi^{(j)},\\ \psi^{(l)} &\longmapsto \psi^{(l)},\end{aligned} \tag{14}$$

where

$$\alpha^{[n],\pm}_{jk} = (2\eta)^{\kappa^{[n]}_{jk}}\sqrt{\frac{2\pi}{\lambda^{[n]}_{jk}}}\frac{c^{\pm}_{jk}}{\Gamma(1 + \kappa^{[n]}_{jk})}e^{i\pi(1/2\mp1)(\kappa^{[n]}_{jk}\mp1/2))} \times\big(\beta^{[n]}_{jk}\big)^{\pm1}(1 + O(\eta^{-1/2})), \tag{15}$$

with

$$c^{+}_{jk} = c_{jk}, \quad c^{-}_{jk} = \overline{c_{jk}}, \quad \kappa^{[n]}_{jk} = \frac{i|c_{jk}|^2}{\lambda^{[n]}_{j,k}}. \tag{16}$$

A brief sketch of the derivation of this connection formula (14) is given in Appendix A.

The constant $\kappa_{jk}^{[n]}$ represents the so-called Landau-Zener parameter at $t = t_{jk}^{[n]}$, and the constant $\beta_{jk}^{[n]}$ is obtained by taking the ratio

$$\beta_{jk}^{[n]} = \gamma_j^{[n]}/\gamma_k^{[n]}, \tag{17}$$

where $\gamma_j^{[n]}$ and $\gamma_k^{[n]}$ represent coefficients connecting WKB solutions $\psi^{(j)}$ and local WKB solutions $\psi^{[n],(j)}$ as

$$\psi_0^{[n],(j)} = \gamma_j^{[n]}\psi^{(j)}, \quad \psi_0^{[n],(k)} = \gamma_j^{[n]}\psi^{(k)}. \tag{18}$$

Here local WKB solutions are introduced as

$$\begin{aligned}\psi_0^{[n],(j)} &= \eta^{-1/2}\exp\left\{\frac{\eta}{i}\int_{t_{jk}^{[n]}}^{t}\rho_j(t')dt'\right.\\ &\quad + \frac{1}{i}\int_{t_{jk}^{[n]}}^{t}\left[|c_{jk}|^2\left(\frac{1}{\rho_j-\rho_k}+\frac{1}{\lambda_{jk}^{[n]}\left(t-t_{jk}^{[n]}\right)}\right)\right.\\ &\quad \left.\left.+\frac{|c_{jl}|^2}{\rho_j-\rho_l}\right]dt'\right\}\left(\frac{\lambda_{jk}^{[n]}\left(t-t_{jk}^{[n]}\right)^2}{2}\right)^{\frac{\kappa_{jk}^{[n]}}{2}}\\ &\quad \times\left(e^{(j)}+O(\eta^{-1/2})\right),\end{aligned} \tag{19}$$

$$\begin{aligned}\psi_0^{[n],(k)} &= \eta^{-1/2}\exp\left\{\frac{\eta}{i}\int_{t_{jk}^{[n]}}^{t}\rho_j(t')dt'\right.\\ &\quad + \frac{1}{i}\int_{t_{jk}^{[n]}}^{t}\left[-|c_{jk}|^2\left(\frac{1}{\rho_j-\rho_k}+\frac{1}{\lambda_{jk}\left(t-t_{jk}^{[n]}\right)}\right)\right.\\ &\quad \left.\left.+\frac{|c_{kl}|^2}{\rho_k-\rho_l}\right]dt'\right\}\left(\frac{\lambda_{jk}^{[n]}\left(t-t_{jk}^{[n]}\right)^2}{2}\right)^{-\frac{\kappa_{jk}^{[n]}}{2}}\\ &\quad \times\left(e^{(k)}+O(\eta^{-1/2})\right).\end{aligned} \tag{20}$$

In actual numerical calculations, not necessarily for the MLZ model, but for the nonlinear model, it is important to find the ratio $\beta_{jk}^{[n]}$, so we in Appendix B provide a concrete recipe to obtain $\beta_{jk}^{[n]}$.

We make a couple of remarks. First, as seen in the derivation in Appendices A and B, the extension to the system with more than three states could straightforwardly be made as far as the reality condition (7) is satisfied. Second, we have not assumed the degree of polynomials $\rho_j(t)$ $(j = 1, 2, 3)$, meaning that WKB solutions and the associated connection formula can be used even in the case where some of or all of $\rho_j(t)$ are nonlinear functions of t. This means that the argument is far beyond the MLZ model. Third, the WKB solutions $\psi^{(j)}$ $(j = 1, 2, 3)$, combined with connection formulas (14), provide the solutions for the original system (3) within the WKB solution, so they can serve as solutions for initial value problems. One of the major goals in the nonadiabatic transition problem would be to gain an explicit expression for the S matrix. This is also possible in the above framework as we already mentioned, but the formula will go beyond that. Given an arbitrary initial population for each state, one can calculate the final population at any time. Such calculations are actually performed in the subsequent sections to see the validity of the WKB formula derived in this way.

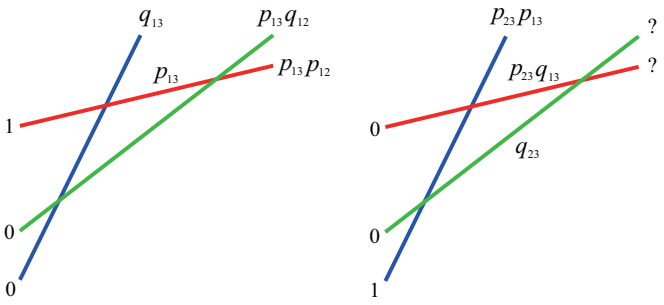

FIG. 1. Diabatic energy levels for the three-state model (schematic). Left: Initial population is given only for the red-colored state. Right: Initial population is given only for the blue-colored state.

III. NUMERICAL VERIFICATION FOR CASES SATISFYING THE REALITY CONDITION

As explained in the previous section, a closed WKB solution and the associated connection formula has been obtained based on the exact WKB analysis. In particular, under the reality condition (7), one finds an explicit expression for the S matrix and even solutions for the initial value problem. Furthermore, the formula covers not only the MLZ model in general situations but also the cases with nonlinear diabatic levels, and hence it is worth testing the obtained WKB formula in various multistate models.

Below we numerically check how the formula works and in which situations it breaks. The reason for why it could break is that we here examine the validity of the leading order WKB formula with respect to $\eta^{-1} = \hbar$. Remember that the exact WKB analysis has provided not only the leading order but higher order terms, so we could go further if the leading order approximation does not work. Such a task asking the validity of higher order approximation is, however, out of the scope of the current study.

A. Independent crossing approximation

Before going to investigating concrete models, we recall an issue that often comes up for debates in the multistate nonadiabatic problem because it is recognized as a point essentially different from two-state problems and might be related with a necessary condition for solvability of the problem.

As was pointed out in [32], when considering multistate nonadiabatic transitions, we are not in general allowed to treat the transition at each crossing point (of diabatic energies) independently, except for some specific cases. When crossing points are well separated, it looks like one can decompose multistate interactions into pairwise ones, which is called *independent crossing approximation* [32]. However, the validity of such a treatment depends on the situation because the relative phase gained in the course of time is significant.

A typical example in which relative phases come into play is illustrated in Fig. 1 [32]. In the left-hand case, only the state shown as a red line is initially populated while other two states (blue and green) are set to be empty. Note that nothing happens at the crossing point between blue and green states since they both have null populations. At the crossing between the red and blue states, some probability transfer

occurs and we suppose that the remaining probability in the red state is given as p_{13}. At the crossing between the red and green states, the green state is empty before interaction, so we do not need to consider the relative phase between the red and green states. Thus, the populations after interaction are unambiguously given as $p_{13}q_{12}$ and $p_{13}p_{12}$, respectively. An independent crossing approximation is expected to work in this situation, and it was actually been confirmed [32].

In the right-hand case, on the other hand, we put a nonzero population only on the blue state. As a result, nonadiabatic transitions occur both at crossing points between the blue and green states, and between the blue and red solid states as well. Then before the crossing point between the red and green states, both states have nonzero populations, so we have to take into account the relative phase between these two states. However, the two-state treatment does not carry any information on the relative phase, so independent crossing approximation cannot apply. This argument implies that the independent crossing approximation might result in an incorrect answer in generic initial population patterns.

B. Linear case

We first examine the validity of our WKB formula when applied to the MLZ model, that is, all the diabatic levels just linearly depend on time:

$$\begin{aligned} \rho_1(t) &= a_1 t + b_1, \\ \rho_2(t) &= a_2 t + b_2, \\ \rho_3(t) &= a_3 t + b_3, \end{aligned} \tag{21}$$

where a_i, b_i $(i = 1, 2, 3)$ are constants and the reality condition (7) is satisfied. In order words, the equation $[\rho_1(t) - \rho_2(t)]\,[\rho_2(t) - \rho_3(t)]\,[\rho_3(t) - \rho_1(t)] = 0$ has three distinct solutions on the real t axis, that is, any pair of levels crosses with each other. Note that there are not any further specific requirements other than these, thus we here discuss the three-level MLZ model in a generic form.

First we show the Stokes geometry, which is indispensable for the WKB analysis. As mentioned in the Introduction, in the case of higher order differential equations, it happens that Stokes curves can cross. When studying the multistate model, it is therefore inevitable to treat such events entirely absent in second-order differential equations.

New objects in the WKB analysis, such as virtual turning points and new Stokes curves for higher order differential equations, are naturally introduced in the exact WKB theory, combined with a general theory of microlocal analysis [53], and will play crucial roles [46,47,51]. However, if the reality condition (7) is fulfilled, it has been proved that we do not have to take into account such new objects when we are interested in calculation of the S matrix or the analytic continuation of WKB solutions along the real axis [37].

We will later provide a precise definition for virtual turning points and new Stokes curves, but we here present an example of the full Stokes geometry for the linear model (21) with the corresponding diabatic energy levels in Fig. 2. As is observed, there actually appear virtual turning points (open green dots) and new Stokes curves (thin dotted and thin solid curves) even if the reality condition (7) is satisfied. When one performs an

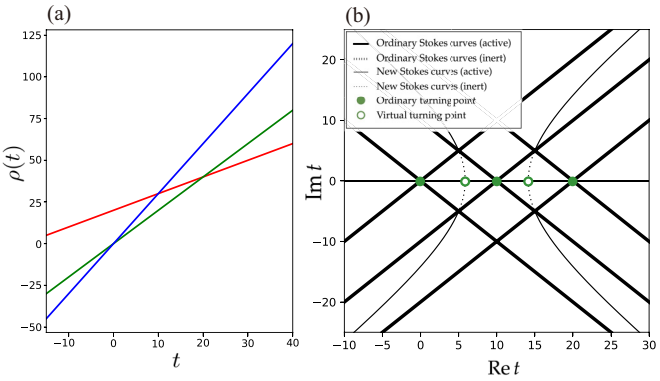

FIG. 2. (a) Diabatic energy levels (21) and (b) Stokes geometry for the model with diabatic energies (21) with $a_1 = 1$, $a_2 = 2$, $a_3 = 3$, $b_1 = 20$, $b_2 = 0$, and $b_3 = 0$. In (b), filled and open green dots are ordinary and virtual turning points. Thick and thin curves are ordinary and new Stokes curves, respectively. Solid and dotted parts in each curve represent active and inert portions of Stokes curves.

analytic continuation of WKB solutions along the real axis, new Stokes curves are inert (dotted portions of thin curves in the figure) in the vicinity of the real axis, which implies that they do not cause any Stokes connections. This example tells us that although virtual turning points and new Stokes curves appear in the Stokes geometry, they do not necessarily contribute to the final output. As will be closely studied below, the issue is totally *global*, meaning that we need a whole set of turning points (ordinary and virtual) and Stokes curves (ordinary and virtual) to complete the connection problem in general, but in the present situation we may pretend that only the ordinary turning points and the ordinary Stokes curves contribute.

Having this in mind, we examine the time evolution of the states for the linear case (21). First note that a final expression for the S matrix has already been presented explicitly (see Eq. (2.42) in [37]). This was obtained as a product of three connection matrices $\widetilde{S} = M_{12}M_{13}M_{23}$, multiplied by normalization constants $N^{(\pm)}$ [see Eq. (9)]. Here connection matrices are respectively expressed as

$$\begin{aligned} M_{12} &= \begin{pmatrix} 1+\alpha_{12}^{-}\alpha_{12}^{+} & -\alpha_{12}^{*} & 0 \\ -\alpha_{12}^{-} & 1 & 0 \\ 0 & 0 & 1 \end{pmatrix}, \\ M_{13} &= \begin{pmatrix} 1+\alpha_{13}^{-}\alpha_{13}^{+} & 0 & -\alpha_{13}^{+} \\ 0 & 1 & 0 \\ -\alpha_{13}^{-} & 0 & 1 \end{pmatrix}, \\ M_{23} &= \begin{pmatrix} 1+\alpha_{13}^{-}\alpha_{13}^{+} & 0 & -\alpha_{13}^{+} \\ 0 & 1 & 0 \\ -\alpha_{13}^{-} & 0 & 1 \end{pmatrix}, \end{aligned} \tag{22}$$

with

$$\begin{aligned} \alpha_{jk}^{\pm} &= c_{jk}^{\pm}\frac{i\sqrt{2\pi}}{\Gamma(1\pm\kappa_{jk})}[e^{\pm i\pi/2}(b_k - b_j)]^{-1/2} \\ &\quad \times (2\eta)^{\pm\kappa_{jk}} e^{(1/2\mp 1)i\pi\kappa_{jk}}\beta_{jk}^{\pm 1}, \\ \kappa_{jk} &= \frac{i|c_{jk}|^2}{b_k - b_j}, \quad c_{jk}^{+} = c_{jk}, \quad c_{jk}^{-} = \overline{c_{jk}}, \end{aligned}$$

and

$$\beta_{12} = e^{i\pi\kappa_{12}}[2(b_2-b_1)]^{-\kappa_{12}}\left(\frac{b_3-b_2}{b_2-b_1}a\right)^{\kappa_{23}-\kappa_{13}} \times e^{i\eta a^2/[2(b_2-b_1)]},$$
$$\beta_{13} = e^{i\pi(-\kappa_{12}+\kappa_{23}+\kappa_{13})}[2(b_3-b_1)]^{-\kappa_{13}} \times \left(\frac{b_3-b_2}{b_3-b_1}a\right)^{-\kappa_{12}-\kappa_{23}},$$
$$\beta_{23} = e^{i\pi\kappa_{23}}[2(b_3-b_2)]^{-\kappa_{23}}a^{\kappa_{12}-\kappa_{13}}. \quad (23)$$

The precise form for M_{12}, M_{13}, and M_{23} is given based on a recipe described in Appendix A, and also a more explicit expression especially to obtain the ratio β_{jk} is given in Appendix B. The connection matrix and thereby the associated S matrix simply take a form of the product of connection matrices in the order of analytic continuation from $t=-\infty$ to $+\infty$ along the real axis. Around each turning point, shown by a green filled dot in Fig. 2, the connection formula

$$(\psi^{(1)}, \psi^{(2)}, \psi^{(3)}) \longmapsto (\psi^{(1)}, \psi^{(2)}, \psi^{(3)})M_{jk} \quad (24)$$

should be applied.

Note here that it looks free from the relative phase problem mentioned above, and one might be even tempted to regard that the independent crossing approximation is valid. However, we recall that a constant β_{jk} is obtained by taking the ratio between WKB solutions $\psi^{(j)}$ and locally reduced ones $\psi_0^{(j)}$, and therefore it depends on the order of analytic continuation. As a result of this fact, as given in (23), we have different expressions for β_{jk} although it is possible to permutate other constants α_{jk}, κ_{jk}, and c_{jk}. In order to see that the relative phase is indeed crucial and at the same time to confirm to what extent the WKB approximation can trace exact time evolutions, we here present some numerical results.

We first demonstrate the case in which only a single state is initially populated and then after some interactions to make the states mixed. In Fig. 3(a) we compare the results obtained using the WKB formula with exact results which are directly obtained by numerical integration of Eq. (3). The initial population pattern is exactly the same as that in Fig. 1(b). We put a nonzero population only in a single state at an initial time t_0, i.e., $[\psi_1(t_0), \psi_2(t_0), \psi_3(t_0)] = (0, 0, 1)$, and the time evolution of the state $\psi_3(t)$ is displayed as a blue curve (numerical integration) and a blue square (WKB calculation), thereby we consider the situation where the independent crossing approximation is not expected to work. It is clearly seen that the WKB solution can quite well trace the exact time evolution, which implies that relative phases among states are properly incorporated in the WKB formula. This holds true even when all the levels are populated initially as shown in Fig. 3(b). Although not shown here, even if we flip the sign of any one of the components or shift the initial time t_0, both leading to totally different time evolution patterns, the WKB formula perfectly reproduces exact numerical integrations. Surprisingly, even for $\eta = 1$, the WKB formula has enough capability of predicting exact results as shown in Fig. 3(c). In the WKB theory, η^{-1} should be a small parameter, which guarantees the validity of the approximation. The effective range can therefore be said to be more than expected.

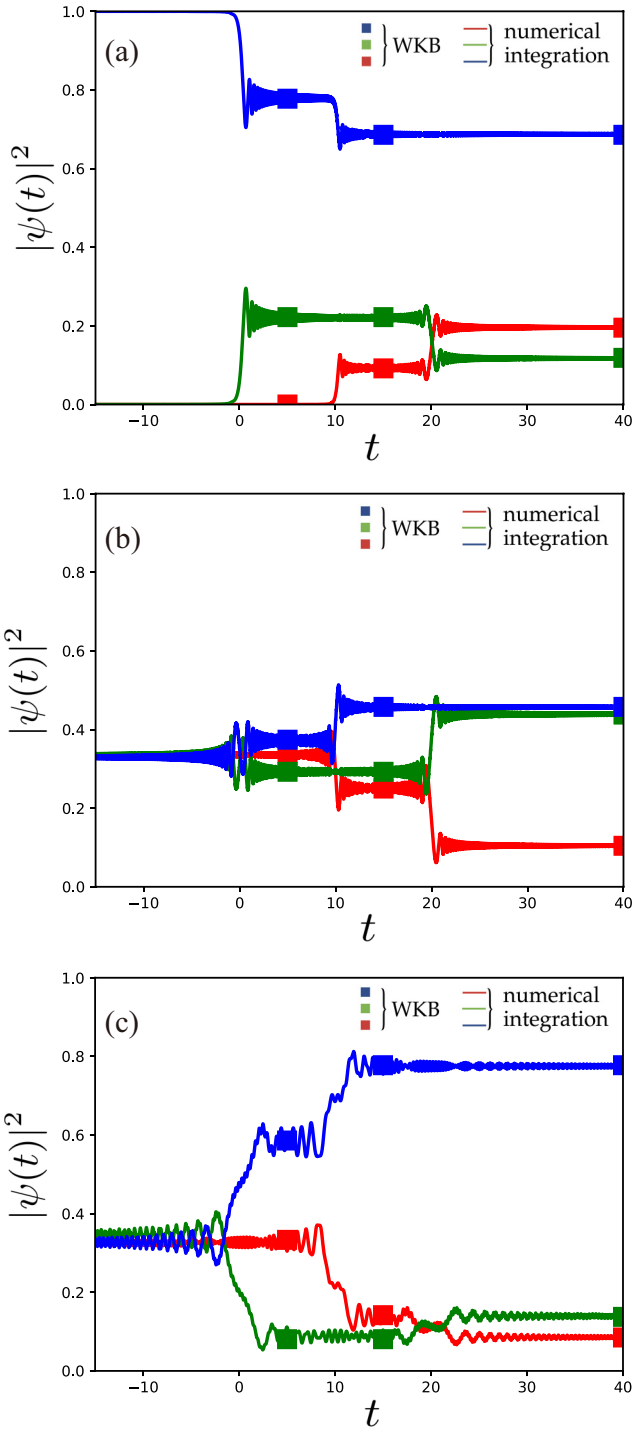

FIG. 3. Comparison between the WKB formula and exact results computed by direct numerical integration of Eq. (3). The parameters are the same as those used in Fig. 2. (a) Initial conditions are taken as $[\psi_1(t_0), \psi_2(t_0), \psi_3(t_0)] = (0, 0, 1)$ where $t_0 = -15$. The inverse Planck constant and off-diagonal elements are given as $\eta = 10$ and $c_{ij} = 0.2$ $(i.j = 1, 2, 3)$. (b) Initial conditions are $[\psi_1(t_0), \psi_2(t_0), \psi_3(t_0)] = (1/\sqrt{3}, 1/\sqrt{3}, 1/\sqrt{3})$ where $t_0 = -15$, and $\eta = 10$ and $c_{ij} = 0.2$ $(1 \leqslant i.j \leqslant 3)$. (c) The sign of the first component in the initial condition is flipped as $[\psi_1(t_0), \psi_2(t_0), \psi_3(t_0)] = (-1/\sqrt{3}, 1/\sqrt{3}, 1/\sqrt{3})$ where $t_0 = -15$, and $c_{ij} = 0.2$ $(1 \leqslant i.j \leqslant 3)$. Note that the large parameter is set to be $\eta = 1$.

This does not, of course, mean that the WKB formula works in every range of parameters. The WKB formula now employed is, as mentioned above, given by taking only the leading order term in the expansion with respect η^{-1}, and so there must exist some limitation for the validity range. As is well known, the leading order WKB approximation breaks in the vicinity of turning points, and this must also be true in the present analysis. If one takes a close look at the region close to each turning point, the WKB formula should fail to reproduce exact results. This sort of breakdown is however not serious and safe in the region far apart from turning points, that is, in the asymptotic regions $t \to \pm\infty$. The results shown in Fig. 3 indeed confirm this argument.

On the other hand, when several turning points come close to each other, the situation changes. In the case where nearly coalescing turning points appear, we need to consider the so-called uniform approximation to overcome the breakdown (see for example [7]). The uniform approximation requires finding an exact solution describing the behavior around coalescing turning points and then connecting with WKB solutions in asymptotic regions.

In the present argument, each turning point has been treated in an independent manner, and degenerated or nearly degenerated situations are out of the scope. Hence the breakdown of the approximation would be expected, and the breakdown brought by near coalescing turning points is indeed observed as shown in Fig. 4. Here we make three diabatic energy levels come close, keeping the off-diagonal matrix elements c_{ij} constant, and compare the results between the WKB formula and numerical integrations. As clearly seen, the WKB prediction gets worse as turning points approach each other. As will be illustrated in Sec. IV, the breakdown due to the coalesce of turning points comes about not only in the case where three turning points degenerate simultaneously as examined here, but also when only two turning points come close to each other.

The breakdown is expected to occur as well when the second term $\eta^{-1/2}H_{1/2}$ in (4) is increased. It would, however, be more subtle in this case since the second term takes a rather unusual form as compared to the standard MLZ model, in which the factor $\eta^{-1/2}$ is not present. As mentioned, this extra factor $\eta^{-1/2}$ was introduced as a result of a formal requirement that the Borel transform and the associated Borel sum of the WKB solution can be defined in a simple form. In the standard off-diagonal form, coupling constants c_{ij} determine the diabaticity(or adiabaticity) of the system: the system is close to the diabatic limit if $c_{ij} \ll 1$, and close to the adiabatic limit if $c_{ij} \gg 1$. In this respect, the results presented in Fig. 3 correspond to the former situation because relatively small off-diagonal couplings c_{ij} multiplied by a rather small value of $\eta^{-1/2}$ were chosen there.

When asking how the WKB formula works in the adiabatic parameter regime, one must increase the product $\eta^{-1/2}H_{1/2}$ in this model, not the value of off-diagonal couplings c_{ij}. We might naively expect that the increase of the product $\eta^{-1/2}H_{1/2}$ will lead to the breakdown of the WKB approximation, but this is not necessarily the case, as actually displayed in Fig. 5. Even though the product $\eta^{-1/2}H_{1/2}$ takes the same value, the result shows that the case with a large value of η better

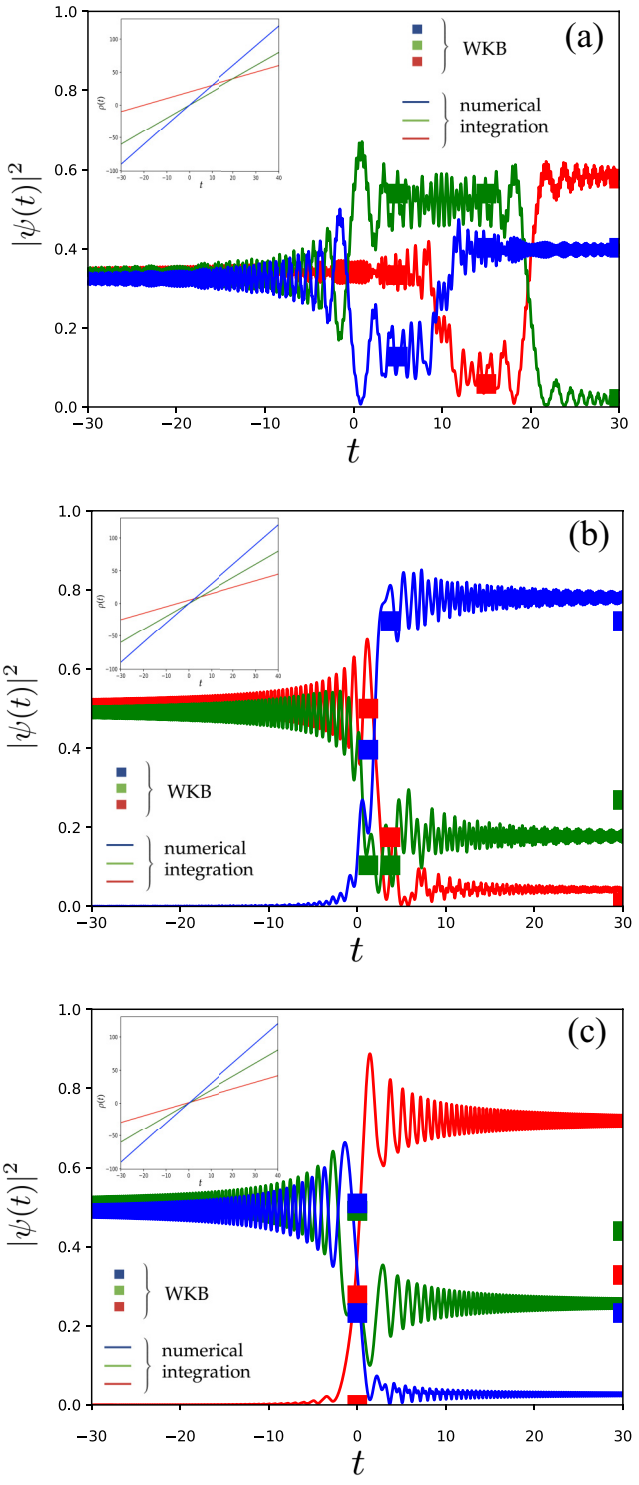

FIG. 4. Comparison between the WKB formula and exact results computed by direct numerical integration of Eq. (3). Exact results and the prediction using the WKB formula are shown as curves and squares, respectively. The diabatic energy levels (21) are given as $\rho_1 = t + b_1$, $\rho_2 = 2t$, and $\rho_3 = 3t$ with (a) $b_1 = 20$, (b) $b_1 = 5$, and (c) $b_1 = 0.01$ (see insets). The inverse Planck constant and off-diagonal elements are given as $\eta = 1$ and $c_{ij} = 0.5$ $(i, j = 1, 2, 3)$. Initial conditions are respectively set as $[\psi_1(0), \psi_2(0), \psi_3(0)] =$ (a) $(1/\sqrt{3}, 1/\sqrt{3}, 1/\sqrt{3})$, (b) $(1/\sqrt{2}, 1/\sqrt{2}, 0)$, and (c) $(0, 1/\sqrt{2}, 1/\sqrt{2})$, respectively.

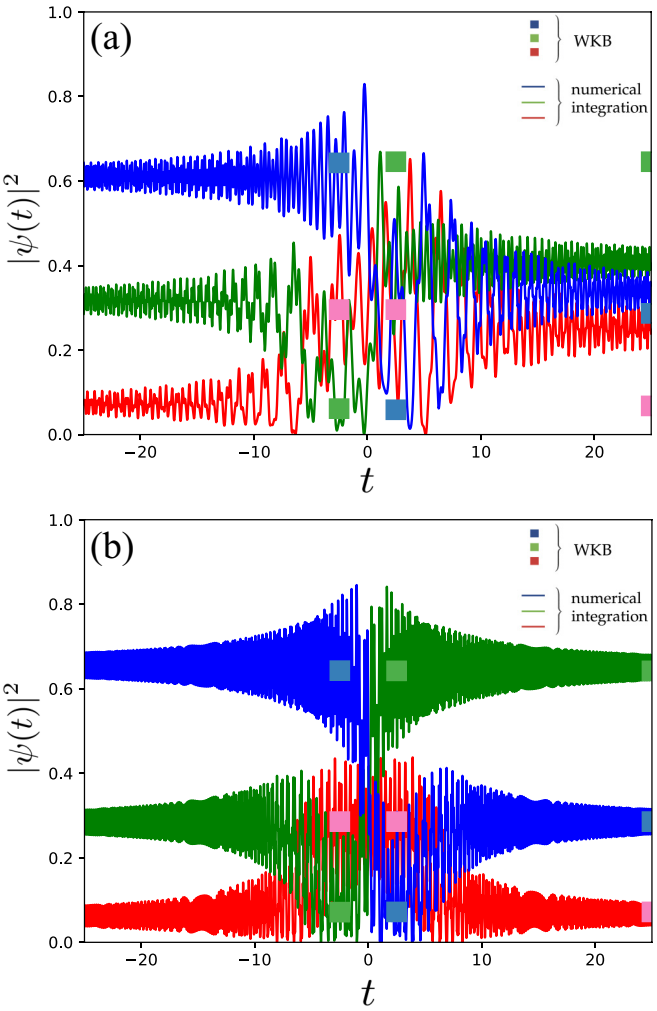

FIG. 5. Comparison between the WKB formula and exact results computed by direct numerical integration of the model (3). Exact results and the prediction using the WKB formula are shown as curves and squares in the figure. The coefficients for the diabatic energy levels (25) are given as $a_1 = 0$, $a_2 = 0$, $b_1 = 0$, $b_2 = -1$, $b_3 = 1$, $c_1 = 5$, $c_2 = 0$, and $c_3 = 0$. (a) Initial conditions are $[\psi_1(t_0), \psi_2(t_0), \psi_3(t_0)] = (-1/\sqrt{14}, -2/\sqrt{14}, -3/\sqrt{14})$ where $t_0 = -25$. The inverse Planck constant and off-diagonal elements are set to be $\eta = 1$ and $c_{ij} = 1.0$ $(1 \leqslant i.j \leqslant 3)$, respectively. (b) Initial conditions are $[\psi_1(t_0), \psi_2(t_0), \psi_3(t_0)] = (1/\sqrt{14}, 2i/\sqrt{14}, -3/\sqrt{14})$ where $t_0 = -25$. The inverse Planck constant and off-diagonal elements are set to be $\eta = 4$, $c_{ij} = 2$ $(1 \leqslant i.j \leqslant 3)$, respectively.

reproduces the exact result compared to the small η case. This would be a reasonable result because the WKB expansion is a series with respect $\eta^{-1/2}$. One should say, therefore, that the validity of the WKB approximation in the adiabatic parameter region depends on the value of η. It is at the same time true that as the product $\eta^{-1/2}H_{1/2}$ becomes larger as a whole, the WKB result should start to deviate from the exact one.

C. Nonlinear case

We now proceed to the case where diabatic energy levels depend on time not linearly but nonlinearly. This is well beyond most of the studies so far available, but, in view of the WKB analysis developed in [37], it adds nothing essential to the treatment. We here examine the case in which two of diabatic energies change quadratically in time and the rest linearly:

$$\begin{aligned} \rho_1(t) &= a_1 t^2 + b_1 t + c_1, \\ \rho_2(t) &= a_2 t^2 + b_2 t + c_2, \\ \rho_3(t) &= b_3 t + c_3. \end{aligned} \tag{25}$$

We stress again that the reality condition (7) is satisfied below, leading to six ordinary turning points in total in the corresponding Stokes geometry.

Following the recipe for locating turning points and drawing the associated Stokes curves emanating from each turning point, together with virtual turning points and new Stokes curves, the latter being closely explained in the next section, we show in Fig. 6 the Stokes geometry for the nonlinear model with diabatic levels (25). Note that explicit and concrete procedures are given in [37] in the case with two linear and one quadratic energies.

The Stokes geometry becomes slightly intricate compared to the linear case, but because of the reality condition, we have only to apply successively the connection formula introduced in Sec. II B, without any consideration of new objects, enabling us to write down the corresponding S matrix if we wish. To obtain explicit expressions for connection matrices M_{12}, M_{13}, and M_{23}, we again use a recipe given in Appendix A, together with a concrete formula presented in Appendix B.

As shown in Fig. 7, the WKB formula again provides extremely good predictions for exact time evolutions. As is the linear case, it works even for $\eta = 1$ as given in Fig. 7(b). The range of validity and aspects of breakdown of the approximation is essentially the same as the linear case. That is, as turning points come close together, the WKB prediction becomes less accurate compared to situations where they are well separated. A treatment based on the uniform approximation is required there again, but this is beyond the scope of the present paper.

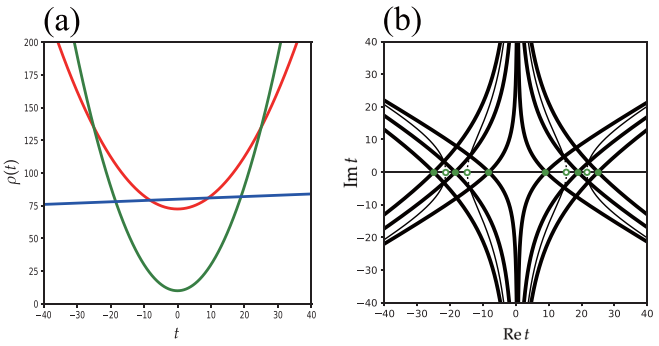

FIG. 6. (a) Diabatic energy levels and (b) the corresponding Stokes geometry. Filled and open green dots are ordinary and virtual turning points. Thick and thin curves are ordinary and new Stokes curves, respectively. Solid and dotted parts in each curve represent active and inert portions of Stokes curves. The coefficients for the diabatic energy levels (25) are given as $a_1 = 0.1$, $a_2 = 0.2$, $b_1 = 0.0$, $b_2 = 0.0$, $b_3 = 0.1$, $c_1 = 72.5$, $c_2 = 10$, and $c_3 = 80$.

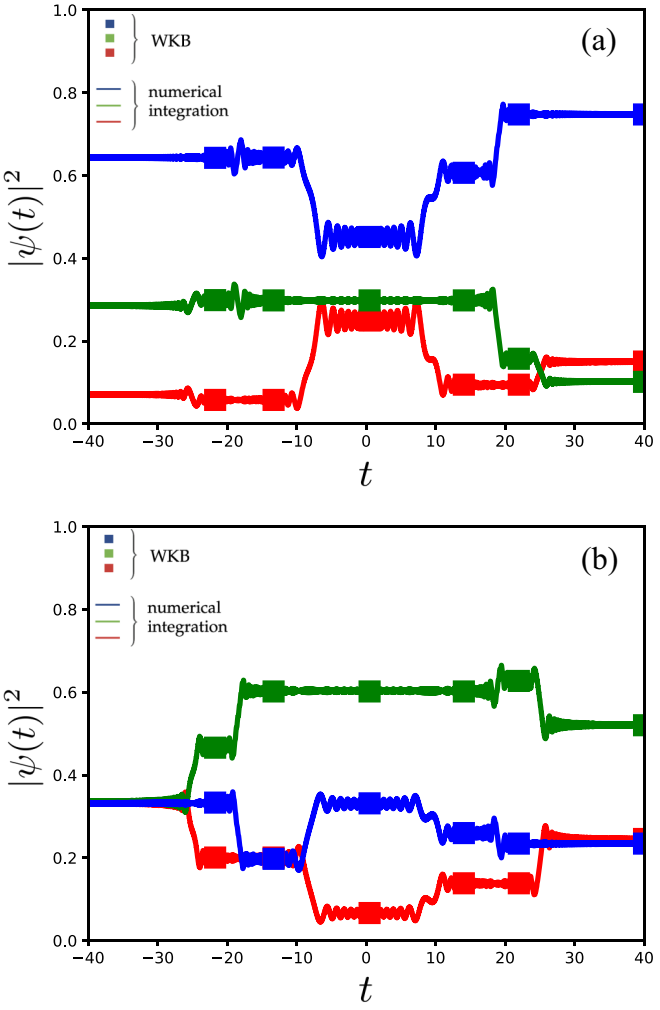

FIG. 7. Comparison between the WKB formula and exact results computed by direct numerical integration of the model (3). Exact results and the prediction using the WKB formula are shown as curves and squares in the figure. The coefficients for the diabatic energy levels (25) are the same as in Fig. 6. (a) Initial conditions are $[\psi_1(t_0), \psi_2(t_0), \psi_3(t_0)] = (1/\sqrt{14}, 2i/\sqrt{14}, -3/\sqrt{14})$ where $t_0 = -40$. The inverse Planck constant and off-diagonal elements are set to be $\eta = 1$ and $c_{ij} = 0.2$ $(1 \leqslant i.j \leqslant 3)$, respectively. (b) Initial conditions are $[\psi_1(t_0), \psi_2(t_0), \psi_3(t_0)] = (1/\sqrt{3}, 1/\sqrt{3}, 1/\sqrt{3})$ where $t_0 = -40$. The inverse Planck constant and off-diagonal elements are set to be $\eta = 1$ and $c_{ij} = 0.2$ $(1 \leqslant i.j \leqslant 3)$, respectively.

IV. ROLE OF VIRTUAL TURNING POINTS AND NEW STOKES CURVES

A. Definition for virtual turning points and new Stokes curves

As stated in Sec. III B, if the reality condition (7) holds, we only need turning points and Stokes curves in the ordinary sense, which are introduced in the traditional asymptotic analysis. Although, as seen in Fig. 2, some of Stokes curves actually cross with each other and a nontrivial situation already comes about in the Stokes geometry, it is not necessary to take into account new objects provided that the reality condition (7) is satisfied. We will provide a more explicit statement given in [37] after introducing new objects in the Stokes geometry.

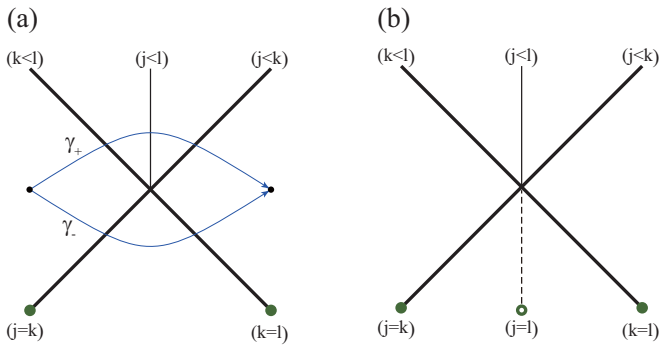

FIG. 8. Crossing of Stokes curves emanating from ordinary turning points (green filled circles). (a) A new Stokes curve emanates from the crossing point, whereas (b) a new Stokes curve emanates from a virtual turning point (green open circle) and passes through the crossing point. Solid and dotted lines represent portions of active and inert Stokes curves, respectively.

Below we give a reasoning to introduce virtual turning points and new Stokes curves in a rather intuitive way. A mathematical background and their rigorous foundation are comprehensively explained in [51]. First we will explain why a new Stokes curve has to be introduced. As seen in Fig. 2, it happens that ordinary Stokes curves cross when they are drawn by following the definition (12). Note that crossing of Stokes curves only occurs in the case of higher order differential equations, not in the second order case. If one performs the connection around a crossing point only by considering Stokes curves drawn under the ordinary rule, the results depend on the path one takes.

To be more concrete, let α_{jk} and α_{kl} be the Stokes coefficients associated with the Stokes curves denoted by $\mathcal{C}_{jk}$ and $\mathcal{C}_{kl}$, respectively, and assume the dominance relation for each Stokes curve, which is put in Fig. 8(a). Under this setting, starting with a solution ψ_l, which is assumed to be the most dominant solution around the crossing point, and following the path denoted by γ_+, one first finds the connection

$$\psi_l \mapsto \psi_l + \alpha_{kl}\psi_k$$

across the Stokes curve $\mathcal{C}_{kl}$, and then the connection

$$\psi_k \mapsto \psi_k + \alpha_{jk}\psi_j$$

follows when passing across the Stokes curve $\mathcal{C}_{jk}$, resulting in

$$\psi_l \mapsto \psi_l + \alpha_{kl}(\psi_k + \alpha_{jk}\psi_j).$$

On the other hand, the connection along the lower path γ_- yields

$$\psi_l \mapsto \psi_l + \alpha_{kl}\psi_k.$$

However, since there exist no singularities around the crossing point, this is a contradiction if $\alpha_{jk}\alpha_{kl} \neq 0$ holds. Alternatively stated, the single valuedness around the crossing point is violated as it stands.

In order to resolve this paradoxical situation around a crossing point, Berk, Nevins, and Roberts have proposed in Ref. [45] to introduce a new Stokes curve $\mathcal{C}_{jl}$ of type $(j < l)$ emanating from the crossing point under consideration [see Fig. 8(a)]. If the coefficient $-\alpha_{jk}\alpha_{kl}$ is attached to such

a newly inserted Stokes curve, the violation of the single valuedness turns out to be avoided.

It might be reasonable to consider a Stokes curve with type (j,k), not only types (j,l) and (k,l) because we have three WKB solutions, and they should be treated on equal footing. However, the origin of a new Stokes curve introduced in such an ad-hoc manner is not clear enough, and it is not obvious whether we may apply it generally. The conventional WKB analysis got stuck there and could not go a step further since there have not been any principle for the Stokes phenomenon for higher order differential equations. Until the exact WKB analysis was developed, no one knew even a rigorous definition of the Stokes phenomenon even in the second order differential equations, so the situation for higher order differential equations is even worse. This has been hampering the WKB analysis for the multistate nonadiabatic transition problem. The analysis based on the Borel summation combined with microlocal analysis made it possible to develop the WKB theory for higher order differential equations and provide a justification for the proposal made in Ref. [45].

In the exact WKB analysis, the Borel transformation of a WKB solution is considered so that singularities on the Borel plane play essential roles and control the Stokes phenomenon. It is therefore natural to consider the Borel transform of a differential operator, say P, which gives rise, in general, to a partial differential operator P_B. Since the Stokes phenomenon is controlled by the singularities on the Borel plane, the observation on the carrier of the singularities for P_B becomes crucial. On the basis of a general theory established in the microlocal analysis [53], one can claim that the so-called bicharacteristic strip is the most elementary carrier of the singularities of solutions of the equation $P_B u = 0$. Here the bicharacteristic strip is a curve generated by the Hamiltonian-Jacobi equation associated with the operator P_B.

In this setting, a turning point in the ordinary sense can be defined as a point at which two cognate singularities on the bicharacteristic curve appear as a confluent point [see Fig. 9(a1)]. Here a bicharacteristic curve is defined as the projection of a bicharacteristic strip onto the coordinate plane (base plane) of the Hamiltonian-Jacobi equation. It is important to note that the behavior of a bicharacteristic curve becomes singular not only at such confluent points in the curves but also self-intersection points [see Fig. 9(b1)]. As a result of this fact, one might expect that a self-intersection point of the bicharacteristic curve bears significant meaning in the exact WKB analysis as a confluent point does so. In fact, a new Stokes curve proposed in Ref. [45] is a Stokes curve emanating from such a point. For this reason a self-intersection point of a bicharacteristic curve should play a similar role as a turning point in the ordinary sense. Ordinary turning points are the points at which the sign of the momentum flips so a particle actually turns, while at a self-intersection point of a bicharacteristic curve nothing turns. The name of a virtual turning point has been put to such a characteristic point [46,47,51]. A new Stokes curve found in Ref. [45] is naturally introduced as a Stokes curve emanating from a virtual turning point.

From a local analysis, it is easy to see that only two Stokes curves emanate from each virtual turning point, whereas three Stokes curves always appear in the vicinity of an ordinary turning point as illustrated in Figs. 9(a2) and 9(b2). As

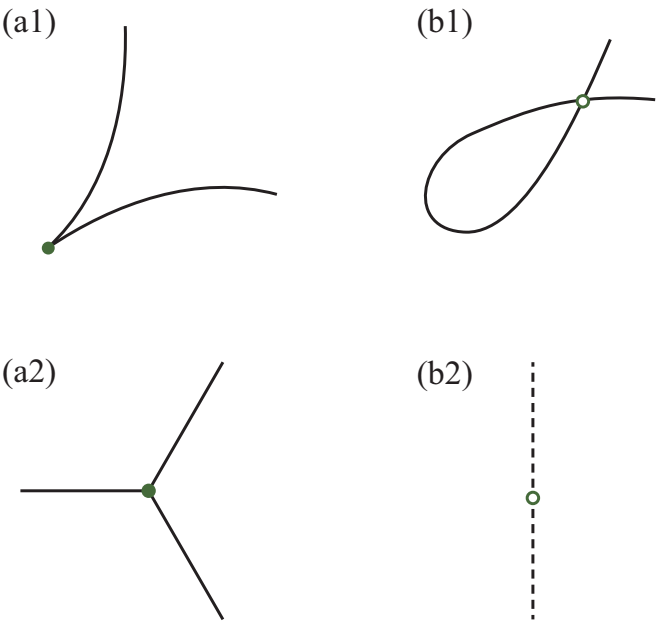

FIG. 9. Illustration of a bicharacteristic curve and associated with (a1) an ordinary turning (green filled circle) point and (b1) a virtual turning point (green open circle). An ordinary turning point appears as a cuspidal point on the bicharacteristic curve, whereas a virtual turning point as a self-intersection point. The corresponding Stokes geometry near (a2) an ordinary turning point and (b2) a virtual turning point. Solid and dotted lines represent an active and inert Stokes curve, respectively.

presented in Ref. [51], it is also possible to prove that no Stokes phenomena are observed when one passes across a new Stokes curve in the vicinity of a virtual turning point [see Fig. 9(b2)]. This fact could be also deduced from the single-valuedness requirement for the WKB solutions around a virtual turning point. If new Stokes curves were active, either of them or both, in the vicinity of a virtual turning point, the WKB solutions could not be single valued. The origin for the name "virtual" comes from the fact that Stokes phenomena do not happen even though a virtual turning point play the role of the point of origin for Stokes curves.

Here we present a more explicit definition for virtual turning points in our multistate nonadadiabatic transition model (3). If a Stokes curve $\mathcal{C}_{jk}$ of type (j,k) that emanates from a turning point t_{jk} crosses with another Stokes curve $\mathcal{C}_{kl}$ emanating from a turning point t_{kl}, and satisfies the relation

$$\int_{t_{jk}}^{t_*} \rho_j(t)dt = \int_{t_{jk}}^{t_{kl}} \rho_k(t)dt + \int_{t_{kl}}^{t_*} \rho_l(t)dt \tag{26}$$

for a mutually distinct (j,k,l), then t_* becomes a virtual turning point for the system (3) and Stokes curves $\mathcal{C}_{jl}$ emanating from the virtual turning point t_* with type (j,l) passes through the crossing point of the Stokes curves $\mathcal{C}_{jk}$ and $\mathcal{C}_{kl}$.

The procedure to find virtual turning points does not stop because it happens that the new Stokes curve obtained in this way may cross with another Stokes curve. For example, suppose that a new Stokes curve $\mathcal{C}_{jl}$ thus obtained intersects with a Stokes curve, say $\mathcal{C}'_{jk}$, emanating from a turning point $t'_{jk} \neq t_{jk}$, then we can associate a virtual turning point t_{**} with

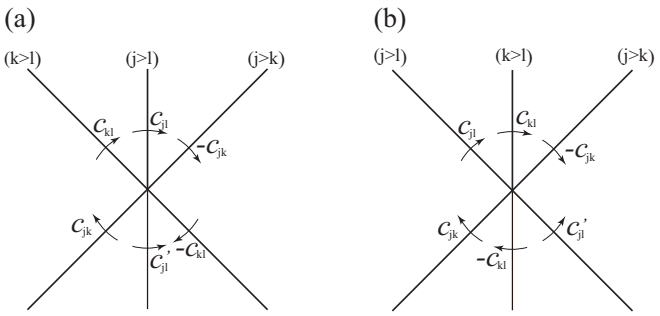

FIG. 10. Two types of relative location achieved at an ordered crossing point. The direction of the connection is attached by the arrow. Each curve can be either an ordinary or a new Stokes curve.

the crossing point of the Stokes curves $\mathcal{C}_{jl}$ and $\mathcal{C}'_{jk}$ through the relation

$$\int_{t'_{jk}}^{t_{**}} \rho_k(t)dt = \int_{t'_{jk}}^{t_{jk}} \rho_j(t)dt + \int_{t_{jk}}^{t_{kl}} \rho_k(t)dt + \int_{t_{kl}}^{t_{**}} \rho_l(t)dt. \tag{27}$$

The relation (26) and also (27) is used to compute virtual turning points numerically.

B. A recipe for finding the Stokes geometry

As explained in the previous subsection, virtual turning points and new Stokes curves are indispensable elements for the WKB analysis of higher order differential equations because crossing of Stokes curves is a generic phenomenon and such new ingredients are necessary to resolve the violation of the single valuedness of the WKB solutions. A set of turning points, ordinary and virtual, together with Stokes curves emanating from either of them, and information on the status of Stokes curves, active or inert is referred to as the Stokes geometry associated with a given differential equation. A concrete recipe to construct the Stokes geometry is summarized as follows:

(i) Draw Stokes curves emanating from an ordinary turning point. They are all active in the vicinity of the associated ordinary turning point.

(ii) Draw new Stokes curves emanating from a virtual turning points. They are inert in the vicinity of the associated virtual turning point.

(iii) If the Stokes curves intersect with each other to form an *ordered crossing point*, the following rule for the Stokes coefficient on each Stokes curves should be applied. There are two possible relative locations of Stokes curves, as shown in Fig. 10, and in either case, due to the single-valuedness requirement, the Stokes coefficients should satisfy the relation

$$\alpha_{jk}\alpha_{kl} + \alpha_{jl} = \alpha'_{jl}, \tag{28}$$

where α_{jk}, α_{kl}, α_{jl}, and α'_{jl} are Stokes coefficients associated with the corresponding Stokes curves (see Fig. 10). Here an ordered crossing point is referred to as a crossing point of the Stokes curve of type (j, k) and (k, l), satisfying the dominance relation $j > k > l$ or $j < k < l$. If the dominance relation does not meet this condition, we call it *nonordered crossing point*. We also say a crossing point is a nonordered crossing point at which two mutually distinct Stokes curves of type (j, k) and (k', l) with $k \neq k'$ intersect.

When a new Stokes curve emanating from a certain virtual turning point encounters an ordered crossing point and the new Stokes curve is of type $(j < l)$, the associated Stokes coefficient might change from inert to active according to the rule (28). For example, if the other Stokes curves are both ordinary ones with $\alpha_{jk}\alpha_{kl} \neq 0$, then the new Stokes curve of type $(j < l)$ turns to be active after passing through the crossing point [see Fig. 8(b)]. However, if $\alpha_{jk}\alpha_{kl} = 0$ holds at the crossing point, then the new Stokes curve is kept intact, i.e., $\alpha_{jl} = \alpha'_{jl} = 0$, even though it passes through the crossing point. Interestingly enough, it can happen that the Stokes coefficient for an ordinary Stokes curve changes when passing through a crossing point, as actually found in [54,55].

We here make an important remark for our subsequent argument. So far all the Stokes coefficients have been assumed to be well determined and actually used in our numerical calculations in Sec. III. However, this assumption is not always satisfied. Stokes coefficients, which appear in the formulas (A6) and (A7), originate from the connection formula for the Weber equation with a double turning point. In this situation, there exists a single double turning point and four Stokes curves emanating from the turning point tend to infinity. On the other hand, in the Stokes geometry for more general situations, not necessarily in higher order differential equation cases, a Stokes curve emanating from a certain turning point happens to hit another turning point. The exact WKB analysis does not provide a recipe to compute Stokes coefficients in such a degenerated situation because the Borel summability is not guaranteed when turning points are connected by a Stokes curve [51]. In the case where all the ordinary turning points are located on the real axis, which is indeed ensured by the reality condition (7), the degeneracy of Stokes curves in this sense does not happen and so we do not need to cope with anything. However, it is not necessarily the case because the parameters in the model are changed to create the *bifurcation* of the Stokes geometry, and the reality condition does not hold any more. This is exactly the case where new elements of the Stokes geometry, such as virtual turning points and new Stokes curves, might come into play.

C. Resolving degeneracy of Stokes curves and the corresponding connection matrix

We note that virtual turning points appear even in the second order differential equation [46]. However, new Stokes curves emanating from virtual turning points in the second order differential equation cannot be active because ordinary Stokes curves do not cross with each other there. All the virtual turning points and new Stokes curves are redundant and do not play any role in the second order differential equation [51]. In this sense one may say that these new objects could be relevant only in higher order differential equations. Since our main concern throughout this paper is the study of the multistate nonadiabatic transition problem, it becomes of particular significance to examine the role of such new elements in the Stokes geometry. As already stated, if the reality condition (7) is fulfilled, we do not apparently need to consider virtual turning points and new Stokes curves

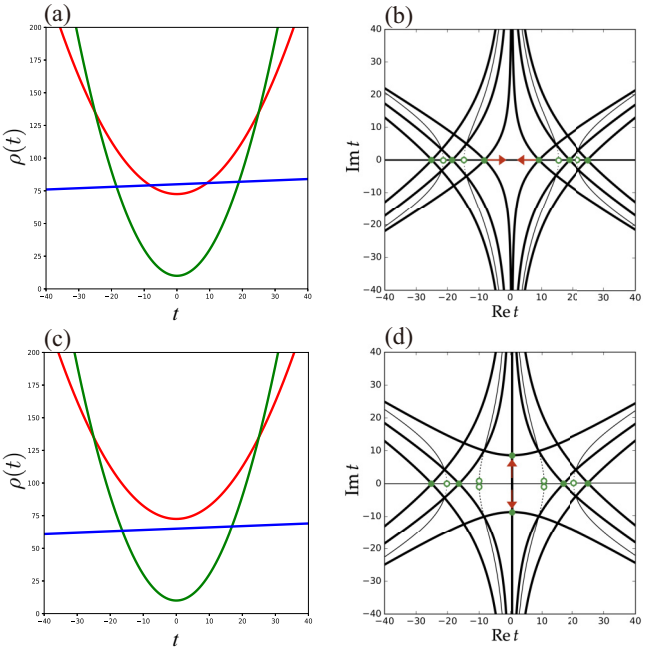

FIG. 11. (a) and (c) Diabatic energy levels (21). (b) and (d) The corresponding Stokes geometry. Filled and open green dots are ordinary and virtual turning points. Thick and thin curves are ordinary and new Stokes curves, respectively. Solid and dotted parts in each curve represent active and inert portions of Stokes curves. Diabatic energy levels are respectively chosen as (a) and (b) $a_1 = 0.1$, $a_2 = 0.2$, $a_3 = 0$, $b_1 = 0$, $b_2 = 0$, $b_3 = 0.1$, $c_1 = 72.5$, $c_2 = 10$, and $c_3 = 80$. (c) and (d) $a_1 = 0.1$, $a_2 = 0.2$, $a_3 = 0$, $b_1 = 0$, $b_2 = 0$, $b_3 = 0.1$, $c_1 = 72.5$, $c_2 = 10$, and $c_3 = 71$.

even though active new Stokes curves appear in the Stokes geometry as seen in Fig. 2. As performed in Sec. III it is enough to proceed along the real axis on which which new Stokes curves are proved to be inert.

As seen in Fig. 11, with the change of a parameter, two of ordinary turning points located on the real axis come close to each other and degenerate at a certain parameter value, and after that they form a complex conjugate pair. The bifurcation of the Stokes geometry thus happens [50,56], and the Stokes geometry is topologically rearranged. Note that the reality condition does not hold any more after the bifurcation.

Since two turning points in the complex plane are connected by a single Stokes curve, we inevitably encounter the degenerated Stokes curve when the WKB solutions are analytically continued along the real axis. Even if a path avoiding the degenerated Stokes curve is found, the connection is affected by the degeneracy because Stokes coefficients around such a turning point are determined by requiring single valuedness of the WKB solution.

As mentioned in the end of the previous section, the exact WKB method cannot handle such a degenerate situation, so we need to build a scheme to overcome it. Here, to apply the connection formula already derived, we resolve the degeneracy of a Stokes curve by adding a small imaginary perturbation $i\varepsilon$ to the diabatic energy levels. As displayed in Fig. 12, depending on the sign of the imaginary perturbation, a degenerated Stokes curve is resolved in two ways.

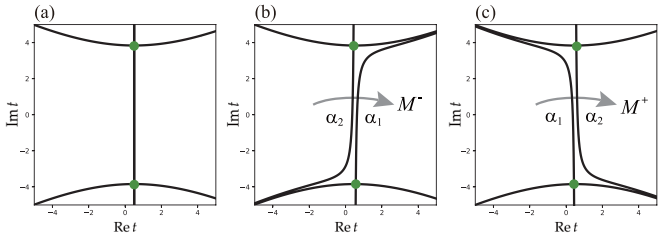

FIG. 12. Magnification of a degenerated Stokes curve shown in Fig. 11. We add a small perturbation $i\varepsilon$ to $\rho_3(t)$ with (a) $\varepsilon = 0$, (b) $\varepsilon = -0.05$, and (c) $\varepsilon = +0.05$.

We now examine how the connection matrices M_+ and M_- behave in the limit of the perturbation parameter $\varepsilon \to 0$. Here, as put in Fig. 12, the matrix M_+ (M_-) represents a connection matrix obtained by adding a positive (resp. negative) perturbation $\varepsilon > 0$ (resp. $\varepsilon < 0$). As is derived in Appendix C, we can show that the Stokes coefficients for the right Stokes curve emanating from the turning point in the lower half-plane and that for the left Stokes curve from the turning point also in the lower half-plane coincide with each other in the limit $\varepsilon \to +0$ and $\varepsilon \to -0$, respectively. In a similar way, the Stokes coefficients for the left Stokes curve emanating from the turning point in the upper half-plane and that for the right Stokes curve also from the turning point in the upper half-plane coincide with each other in the limit $\varepsilon \to +0$ and $\varepsilon \to -0$, respectively.

Let α_1 and α_2 be the limiting values in each case as illustrated in Fig. 12, and examine the connection matrices M_+ and M_-. The formulas for Stokes coefficients derived in Appendix C lead to

$$\lim_{\varepsilon\to+0} M_+ = \begin{pmatrix} 1 & -\alpha_1 \\ \alpha_2 & 1-\alpha_1\alpha_2 \end{pmatrix}, \tag{29}$$

$$\lim_{\varepsilon\to-0} M_- = \begin{pmatrix} 1-\alpha_1\alpha_2 & -\alpha_1 \\ \alpha_2 & 1 \end{pmatrix}. \tag{30}$$

Since $\alpha_1\alpha_2 \neq 0$, $\lim_{\varepsilon\to+0} M_+$ and $\lim_{\varepsilon\to-0} M_-$ do not coincide, meaning that the result of connection depends on which direction the degenerated Stokes curve is resolved. It is easy to see that the difference in the S matrix comes from the difference between $\lim_{\varepsilon\to+0} M_+$ and $\lim_{\varepsilon\to-0} M_-$ because of the relations (C6), (C8), and (C10), resulting in the identical connection matrices near irrelevant real turning points and also to the identical WKB solutions in the limit of $\varepsilon \to \pm 0$.

In the resurgent theory a proper way of averaging over two limits has been discussed [43], but here we just observe how much the difference affects the result. For the limit $\varepsilon \to -0$ we have

$$\begin{aligned}\alpha_1\alpha_2 = {} & \eta^{-2\kappa_{jk,-}} \exp\left(-\frac{a\eta}{6}|t_{jk,+} - t_{jk,-}|^3\right) \\ & \times \frac{2\pi|c_{jk}|^2}{\Gamma(1-\kappa_{jk,-})^2}|t_{jk,+} - t_{jk,-}|^{2\kappa_{jk,-}-1} a^{-2\kappa_{jk,-}-1} \\ & \times \prod_{m=1}^{q}(t_{jk,-} - t_{jl,m})^{2\kappa_{jl,m}} \prod_{m=1}^{s}(t_{jk,-} - t_{kl,m})^{-2\kappa_{kl,m}}. \end{aligned} \tag{31}$$

Here $t_{jk,+}$ and $t_{jk,-}$ stand for the location of the turning points in the complex plane, respectively (see Fig. 21). $t_{jl,m}$ ($m =$

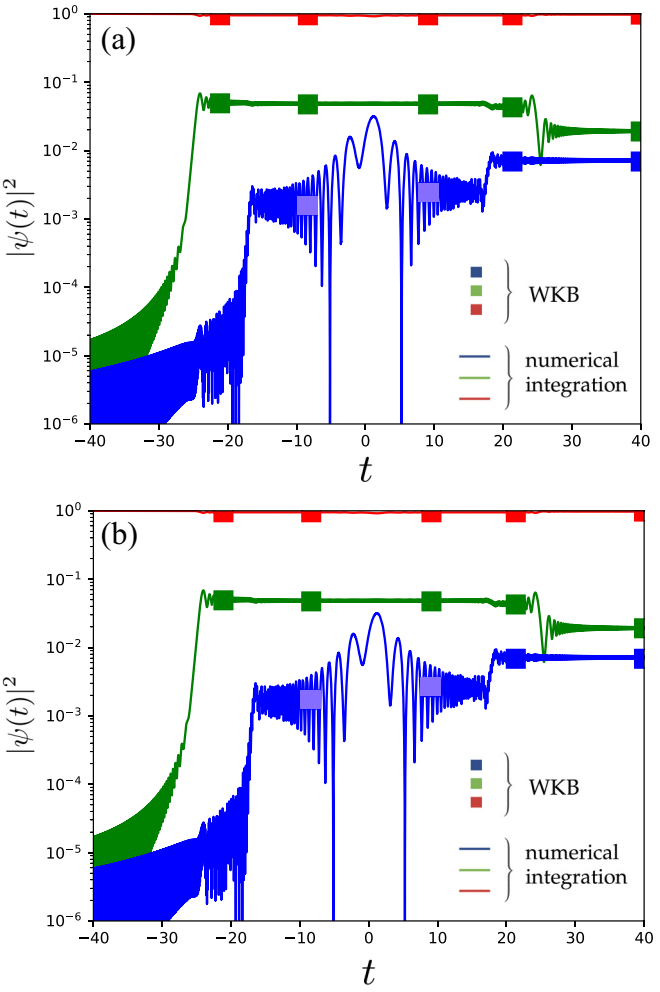

FIG. 13. Comparison between the WKB formula and the results computed by direct numerical integration of the model (3). Diabatic energy levels are shown in Fig. 11. Exact results and the prediction using the WKB formula are shown as curves and squares in the figure. The populations $|\psi(t)|^2$ $(i = 1, 2, 3)$ are plotted in logarithmic scale. The inverse Planck constant and off-diagonal elements are chosen as $\eta = 1$ and $c_{ij} = 0.2$ $(1 \leqslant i.j \leqslant 3)$, and diabatic energy levels are respectively chosen as $a_1 = 0.2$, $a_2 = 0.1$, $a_3 = 0$, $b_1 = 0$, $b_2 = 0$, $b_3 = 0$, $c_1 = 72.5$, $d_2 = 10$, and $d_3 = 71$ with a small perturbation (a) $\varepsilon = 10^{-10}$ and (b) $\varepsilon = -10^{-10}$. Initial conditions is set as $[\psi_1(t_0), \psi_2(t_0), \psi_3(t_0)] = (1, 0, 0)$ where $t_0 = -40$.

$1, \ldots, q)$ and $t_{kl,m}$ $(m = 1, \ldots, s)$ are introduced in (C2) and (C3), representing the position of other turning points located on the real axis and not relevant in the present analysis. Other parameters a, $\kappa_{jk,-}, \kappa_{jl,m}$ $(m = 1, \ldots, r)$, and $\kappa_{kl,m}$ $(m = 1, \ldots, s)$ are also introduced in Appendix C. We obtain a similar expression for $\alpha_1\alpha_2$ for $\varepsilon \to +0$ as well.

Since η is supposed to be a large parameter, the magnitude of the product $\alpha_1\alpha_2$ is exponentially small even though the factor $\eta^{-2\kappa_{jk,-}}$ is present. Also note that with increase of the distance $|t_{jk,+} - t_{jk,-}|$ between complex conjugated turning points, $\alpha_1\alpha_2$ gets smaller. From this observation we would expect that the difference coming from the product $\alpha_1\alpha_2$ is negligible and will not affect the result so much if η is large enough. We can confirm this prediction in Fig. 13. The turning points in question are located in the complex domain, resulting in exponentially small Stokes coefficients for the associated Stokes curves, so the magnitude of the transition itself becomes also exponentially small. For a sufficiently small choice of ε, the discrepancy between the cases with $\varepsilon > 0$ and $\varepsilon < 0$ is negligibly small, and both WKB calculations well predict exact time evolutions.

D. Role of new Stokes curves

As discussed in the previous subsection, some of ordinary turning points fall into the complex plane after the bifurcation, and the reality condition (7) is no longer valid. However, this does not necessarily mean that virtual turning points and new Stokes curve immediately start to play a substantial role and affect the final output. As seen in Fig. 11(d), even after the bifurcation new Stokes curves are still inert near the real axis. When the analytic continuation is made along the real axis, we do not encounter any active new Stokes curves in such a situation. The connection is affected only by ordinary Stokes curves passing across the real axis as analyzed above, but the rest of connections follows the same as those before the bifurcation. In order to see the effect of new Stokes curves, it would be necessary to further change the parameters to realize situations where active new Stokes curves pass cross the real axis. We here present two qualitatively different examples in which new Stokes curves become active when they pass across the real axis.

The first example is the case where an active new Stokes curve forms a complete barrier and no loopholes cannot be found in the course of the analytic continuation. Such an example was found in [57] for the system whose diabatic energy levels are given as

$$\begin{aligned} \rho_1(t) &= t^3, \\ \rho_2(t) &= -t, \\ \rho_3(t) &= -t + c + c^3, \end{aligned} \tag{32}$$

where c is a parameter, which is chosen in a way to realize a desired Stokes geometry. The diabatic energy curves and the corresponding Stokes geometry are displayed in Figs. 14(a) and 14(b), respectively. The red curve in the Stokes geometry represents a new Stokes curve forming a complete barrier. Without passing across it the analytic continuation from $t = -\infty$ to $t = +\infty$ could not be achieved.

In this model, the connection matrix $\widetilde{S}$, a major ingredient for the S matrix (9), is shown to take the form as [57]

$$\widetilde{S} = \begin{pmatrix} 1 & \alpha_1(1 + \widetilde{\alpha}_1\widetilde{\alpha}_2) + \alpha_3\widetilde{\alpha}_1 & \alpha_3 + \alpha_1\widetilde{\alpha}_2 \\ \alpha_2 & (1 + \alpha_1\alpha_2)(1 + \widetilde{\alpha}_1\widetilde{\alpha}_2) & (1 + \alpha_1\alpha_2)\widetilde{\alpha}_2 \\ \alpha_4 & \alpha_1\alpha_4(1 + \widetilde{\alpha}_1\widetilde{\alpha}_2) + (1 + \alpha_3\alpha_4)\widetilde{\alpha}_1 & 1 + \alpha_3\alpha_4 + \alpha_1\alpha_4\widetilde{\alpha}_2 \end{pmatrix}, \tag{33}$$

where α_i $(1 \leqslant i \leqslant 4)$ denote the Stokes coefficients for ordinary Stokes curves and $\widetilde{\alpha}_i$ $(i = 1, 2)$ those for new Stokes curves.

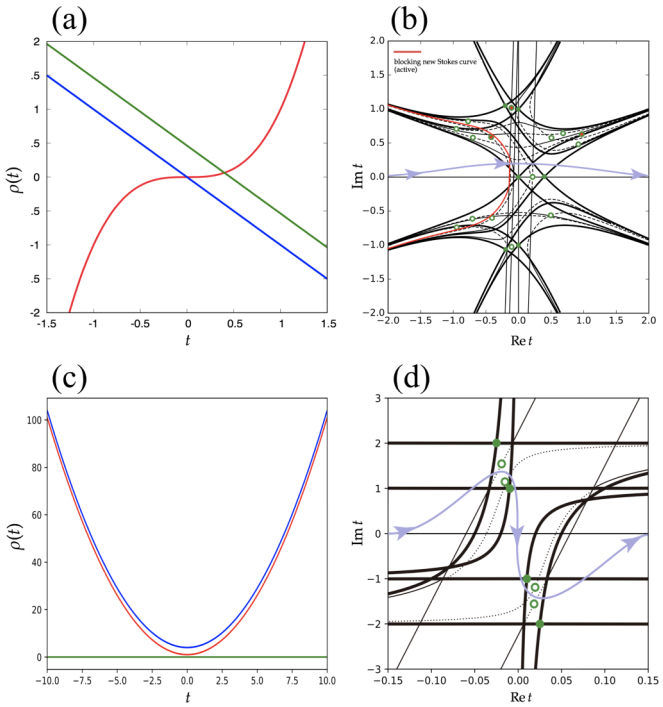

FIG. 14. (a) Diabatic energy curves and (b) the corresponding Stokes geometry for the model (32) with $c = 0.4 + 0.01i$. In (b) the red curve represents the new Stokes curve forming a complete barrier of the analytical continuation. (c) Diabatic energy curves and (d) the corresponding Stokes geometry for the model (34) with $\varepsilon_1 = +0.02$ and $\varepsilon_2 = +0.1$. In (b) the purple curve with arrow stands for a path of the analytical continuation. In (d) the purple curve shows a path avoiding active portions of new Stokes curves. The analytical continuation to calculate the time evolution is actually made by taking a path along the real axis, as is done for the case (b).

As closely studied in [57], a Stokes coefficient associated with a new Stokes curve emanating from a virtual turning point gains an exponentially small factor, which is related to the imaginary part of the virtual turning point. The reason for having an exponential small factor is similar to the case where the ordinary Stokes curves run across the real axis studied above. In the (1,2) element for example, the Stokes coefficients $\widetilde{\alpha}_1$ and $\widetilde{\alpha}_2$, both associated with new Stokes curves, appear in the connection matrix, but the terms $\alpha_1\widetilde{\alpha}_1\widetilde{\alpha}_2$ and $\alpha_3\widetilde{\alpha}_1$ are exponentially small compared to the term α_1, which is the Stokes coefficient for an ordinary Stokes curve emanating from an turning point located in the real axis. As a result, the effect of new Stokes curves is hidden by that of an ordinary curve and so would not be detectable. On the other hand, this is not the case for the (2,3)-element $(1 + \alpha_1\alpha_2)\widetilde{\alpha}_2$, so we might have a chance to make a direct observation of the effect of a new Stokes curve.

The new Stokes curve (in red) forming a complete barrier is a composition of type $(2 < 3)$, type $(1 < 3)$, and type $(2 < 1)$ new Stokes curve, and the connection between the states ψ_2 and ψ_3 occurs when crossing this new Stokes curve. In addition, we notice from the form of the connection matrix (33) that this is exactly a new Stokes curve on which the contribution from the new Stokes curves may be visible. Hence, we examine the visibility of the new Stokes curve by giving the initial condition $(\psi_1, \psi_2, \psi_3) = (0, 0, 1)$.

Figure 15(a) displays the exact time evolution and the result using the WKB formula for the case $\eta = 1$. We first notice that, even though they are plotted in logarithmic scale, there is no visible signature of the transition between state 3 (blue) and state 2 (green) in the exact time evolution. They only exhibit oscillatory patterns but there is no significant difference in average before and after the transition. This is because the diabatic curves $\rho_2(t)$ and $\rho_3(t)$ are running in parallel, which gives rise the observed behavior of the exact time evolution.

Such a specific signature of diabatic levels makes the WKB treatment difficult. Indeed, when applying the WKB calculation for this situation, as seen in Fig. 15(a), we find that the leading order WKB formula does not predict the exact result, for the reason indicated above. Even after passing across a new Stokes curve, which is expected to occur around $t = 0$, the WKB prediction keeps constant while the exact time evolution periodically oscillates. As shown in Fig. 15(b), the situation is almost the same in case of $\eta = 10$. The states 2 and 3 stay constant with periodic oscillation in exact time evolutions, whereas the WKB calculation does not work as in the case of $\eta = 1$.

The second example is the case where active new Stokes curves run across the real axis, but active portions do not form a complete barrier but limited only close to the real axis. In this case it is possible to find an analytical continuation path avoiding active portions of the new Stokes curves and to follow a path passing only through ordinary Stokes curves. The diabatic energies of such a situation found in [58] are given as

$$\begin{aligned} \rho_1(t) &= t^2 + 1 + i\varepsilon_1, \\ \rho_2(t) &= 0, \\ \rho_3(t) &= t^2 + 4 + i\varepsilon_2, \end{aligned} \tag{34}$$

where the constants ε_1 and ε_2 are properly chosen to realize a desired situation. The diabatic potential curves and the corresponding Stokes geometry are displayed in Figs. 14(c) and 14(d), respectively. As inserted in Fig. 14(d), we can find a path avoiding active portions of new Stokes curves, which is displayed by a purple curve with arrows. In this case, new Stokes curves are apparently irrelevant and do not play a role. It should be noted, however, that we do need the information on where new Stokes curves are running and in which portions they are active. In other words, to find such a loophole in the path of the analytic continuation, we need complete information for virtual turning points and new Stokes curves. If the analytical continuation is simply made along the real axis without such information, we inevitably encounter active new Stokes curves. In this sense we should say that active new Stokes curves definitely play a role even though they do not form complete barriers.

In this model, the connection matrix $\widetilde{S}$ is shown to take the form as [58]

$$\widetilde{S} = \begin{pmatrix} 1 + \widetilde{\alpha}_1\widetilde{\alpha}_2 & \alpha_2 + \alpha_1\widetilde{\alpha}_2 & \widetilde{\alpha}_2 \\ \alpha_3 + \alpha_4\widetilde{\alpha}_1 & 1 + \alpha_2\alpha_3 + \alpha_1\alpha_4 & \alpha_4 \\ \widetilde{\alpha}_1 & \alpha_1 & 1 \end{pmatrix}, \tag{35}$$

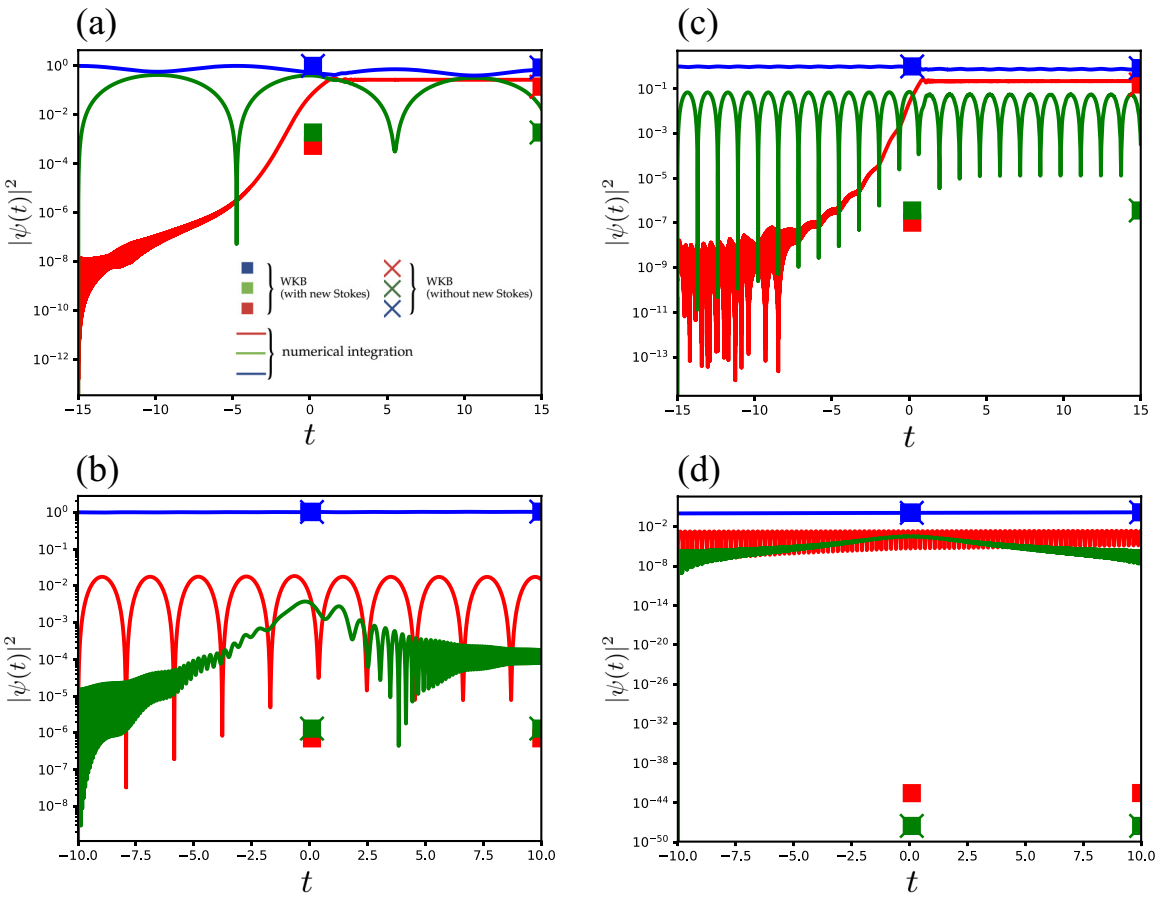

FIG. 15. Comparison between the WKB formula and exact results computed by direct numerical integration. (a) and (b) The results for the model (32) with $c = 0.4 + 0.000001i$. (c) and (d) The results for the model (34) with $\varepsilon_1 = +0.0002$, $\varepsilon_2 = +0.001$. The inverse Planck constant is respectively set to be (a) $\eta = 1$, (b) $\eta = 10$, (c) $\eta = 1$, and (d) $\eta = 10$, and $c_{ij} = 0.2$ $(1 \leqslant i, j \leqslant 3)$ is taken for off-diagonal elements. Exact results and the prediction based on the WKB formula, including new Stokes curves, are shown as curves and squares, respectively, in the figure. The results not including the contribution from new Stokes curves are shown by crosses. The Stokes coefficient for the active new Stokes curve is (a) $5.73 \times 10^{-2} + 2.12 \times 10^{-4}i$, (b) $5.95 \times 10^{-4} + 5.95 \times 10^{-4}i$, (c) $7.98 \times 10^{-5} + 8.72 \times 10^{-4}i$, and (d) $5.48 \times 10^{-23} + 4.86 \times 10^{-22}i$. The red, green, and blue colored curves, respectively, display the time evolution for $|\psi_1|^2$, $|\psi_2|^2$, and $|\psi_3|^2|$. Initial conditions is set as $[\psi_1(t_0), \psi_2(t_0), \psi_3(t_0)] = (0, 0, 1)$ where $t_0 = -10$.

where α_i $(1 \leqslant i \leqslant 4)$ again denote the Stokes coefficients for ordinary Stokes curves and $\widetilde{\alpha}_i$ $(i = 1, 2)$ those for new Stokes curves.

In this case, as was found in [58], the magnitude of $\widetilde{\alpha}_2$, (1,3) element in the connection matrix is much larger than α_4, (2,3) element in the connection matrix, implying that the effect of the new Stokes curve associated with $\widetilde{\alpha}_2$ might be detectable.

This is also a chance to directly observe the contribution from new Stokes curves. However, as demonstrated in Figs. 15(c) and 15(d), there is no visible signature of the transition between state 3 (blue) to state 1 (red) in the exact time evolution. They only exhibit oscillatory patterns and no significant difference in average before and after the transition. This is again because the diabatic curves $\rho_1(t)$ and $\rho_3(t)$ are running in parallel as in the previous example.

These are all known examples so far leading to the possibility to observe explicitly the effect of new Stokes curves. As shown below, there is another example in which any pair of diabatic energy curves do not run in parallel, yet some portions of active new Stokes curves cross the real axis. The diabatic energy levels for such an example are given as

$$\begin{aligned} \rho_1(t) &= c_1, \\ \rho_2(t) &= t + c_2, \\ \rho_3(t) &= t^2 + c_3. \end{aligned} \tag{36}$$

where c_1, c_2, and c_3 are constants. The diabatic energy curves and the corresponding Stokes geometry to realize our desired situation are illustrated in Fig. 16. As in the case of the model (34), we can find a path avoiding the crossing with active portions of the two new Stokes curves, as displayed in Fig. 16(b).

This looks providing an example with visible new Stokes curves. As illustrated in Fig. 17, however, the WKB calculation does not reproduce the exact integration well. The breakdown of the WKB approximation happens, as demonstrated in Fig. 4, when turning points are close to each other. The disagreement seen in Fig. 17 has the same origin. When performing analytical continuation along a real axis, we encounter the two ordinary and two new Stokes curves, all running vertically as seen in Fig. 16(b). However, since

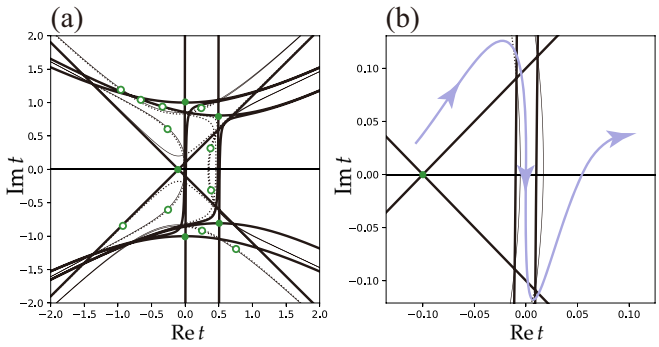

FIG. 16. (a) and (b) Stokes geometry for the model (36) with $c_1 = 1$, $c_2 = 1.1$, and $c_3 = 2 + 0.01i$. (b) A magnification of (a). The purple curve with an arrow shows a path of the analytical continuation avoiding active portions of new Stokes curves.

the ordinary turning points and virtual turning points as well associated with those Stokes curves are relatively close to the real axis. This situation leads to the breakdown of the WKB approximation.

In order to avoid such a situation, we need separate pairs of turning points. However, when turning points, either ordinary or virtual, are located far from the real axis, the amplitude of Stokes coefficients becomes exponentially small, thereby the contribution of new Stokes curves is not expected to be detectable.

This scenario would be generally true: In order to have a relatively large Stokes coefficient, the associated virtual turning point has to be close to the real axis because, as stated above, Stokes coefficients for Stokes curves passing across the real axis are exponentially small in general with respect to both η and the imaginary part of associated virtual points. Our experience tells us that virtual turning points and ordinary turning points move in a correlated way with the change of parameters. This means that ordinary turning points should also have to be close to the real axis. However, if a pair of ordinary Stokes turning points is close to each other, this makes the WKB approximation invalid.

In any case, we have not so far succeeded in finding a model with a proper parameter set, which provides an example with visible new Stokes curves. We should perform a more systematic analysis in order to know how generic or natural visible new Stokes curves happen to appear in physically relevant multistate nonadiabatic transition models.

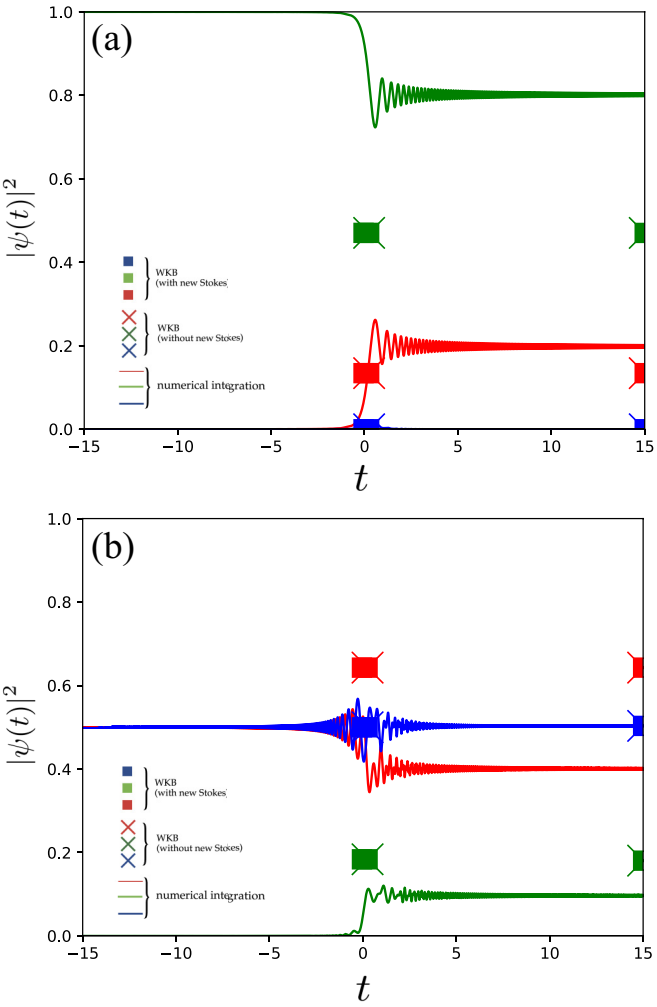

FIG. 17. Comparison between the WKB formula and exact results computed by direct numerical integration of the model (3). Exact results and the prediction based on the WKB formula, including new Stokes curves, are shown as curves and squares, respectively, in the figure. The results not including the contribution from new Stokes curves are shown by crosses. The coefficients for the diabatic energy levels (36) are taken as $c_1 = 1.0$, $c_2 = 1.1$, and $c_3 = 2.0 \times 10^{-10}$. Initial conditions are $[\psi_1(t_0), \psi_2(t_0), \psi_3(t_0)] = (0, 1, 0)$ for (a) and $(1/\sqrt{2}, 0, 1/\sqrt{2})$ for (b), where $t_0 = -20$. The inverse Planck constant and off-diagonal elements are set to be $\eta = 10$ and $c_{ij} = 0.2$ $(1 \leqslant i.j \leqslant 3)$, respectively.

V. SUMMARY AND CONCLUSION

In this paper we have numerically verified the validity of the leading order WKB formula derived based on the exact WKB analysis for three-level nonadiabatic transition model. Since the exact WKB analysis is developed based on the Borel resummation of the WKB expansion, it allows us to get rid of the ambiguity inherent in the divergent series, and as a result of this the Stokes phenomenon, a discontinuous change of the form of WKB solutions, can be reformulated on a firm mathematical footing. In particular, the WKB analysis for higher order differential equations had not been possible until the exact WKB analysis was established. The paper [37] is full of mathematical flavor, and indeed was written to provide a mathematical foundation for the multistate nonadiabatic transition problem. On the other hand, what we intended to perform throughout the paper is to demonstrate that the proposed formula actually works well, which implies that the multistate nonadiabatic transition problem, not necessarily in specific settings but even in generic situations, is now within reach of the WKB approach.

We have mainly examined the three typical typical situations:

(i) Diabatic energy levels depend on linearly on time and all the levels intersect with each other.

(ii) Diabatic energy levels depend on nonlinearly on time and all the levels intersect with each other.

(iii) Diabatic energy levels depend on nonlinearly on time but some of levels do not intersect.

For the first two cases (i) and (ii), the reality condition (7) is satisfied, whereas it does not hold in case (iii).

If the reality condition holds, it has been shown that the WKB formula well predicts the results obtained by direct numerical integration unless turning points nearly coalesce with each other. It should be emphasized that the linearity (nonlinearity) does not matter at all as to whether the formula works or not. Even for the case where all the states are initially populated, the result of the WKB formula is in an excellent agreement with exact time evolutions.

As remarked in Sec. III, however, the success of WKB calculation does not mean that the so-called independent crossing approximation is valid in any situation. It appears that the S matrix is obtained by multiplying connection matrices, which might lead us to speculate that the transition happens independently at each crossing point. However, this is not the case, and the relative phase gained in-between crossing points in fact plays a crucial role. Without taking it into account in an appropriate manner we fail to reproduce correct time evolutions. The WKB formula used here properly incorporates the relative phase and this is the very reason why it works well in arbitrarily chosen conditions.

In the case where the reality condition does not hold, entirely new objects, which appear only in the WKB analysis for higher order differential equations, should be seriously considered. Virtual turning points and new Stokes curves are, as explained in Sec. IV, not only naturally predicted from a general theory of microlocal analysis, but also should inevitably be introduced so that the single valuedness of WKB solutions around a crossing point of Stokes curves is achieved.

We first studied the case where the reality condition is slightly violated and new Stokes curves are still inert in the vicinity of the real axis. Through the bifurcation, it was shown that the topology of the Stokes geometry changes, which gives rise to the situation where two ordinary turning points are connected by a single Stokes curve. The degeneracy of such a kind is known to be beyond the treatment of the exact WKB analysis, so we tried to cope with it by adding a small imaginary perturbation. This results in resolving the degeneracy but as a price we have to pay the connection matrix and the S matrix as well turns out to depend on the sign of the perturbation. We have examined how serious is such a difference in actual numerical predictions and found that the WKB formula still works well as far as the magnitude of the perturbation is small enough. This is due to the fact that the difference arising from perturbation with opposite signs only causes an exponentially small effect with respect to our large parameter η and the distance between complex paired turning points.

As deforming the Stokes geometry further, we encounter the situation where active new Stokes curves pass across the real axis. If we perform the analytic continuation along the real axis, the connection across the active new Stokes curves becomes unavoidable.

There are two possible situations there. The first situation is the case where a complete active new Stokes curve is formed in the Stokes geometry. In this case we cannot avoid taking into account the connection across such a new Stokes curve any more, and such a model has been indeed discovered in Ref. [57]. What is remarkable is not only to show the existence of a new Stokes curve forming a complete barrier, but also to reveal the detectability in the sense of the magnitude. This was done by comparing Stokes coefficients for the associated active new Stokes curve with that for other ordinary Stokes curves, and it was found that in certain situations the former is larger than the latter [58].

Another possibility is that a portion of an active Stokes curve passes across the real axis. but does not necessarily form a complete barrier, meaning that a properly chosen analytic continuation path can be found without passing through active portions of new Stokes curves [57,59]. As a result new Stokes curves apparently do not play any role. However, even in such a situation, we need to prepare information on new Stokes curves with the status, either active or inert, because without such data we could not find a path avoiding active new Stokes curves. For this reason we may say that new objects are crucial to construct the S matrix of the system.

In the present paper we took these two cases in order to see the visibility of new ingredients in the nonadiabatic transition problem. However, as was presented and pointed out in Sec. IV D, due to a specificity of the models proposed in Refs. [57,58], it was not possible to find a clear signature of the contribution from new Stokes curves. In both models, the expected transition across new Stokes curves occurs between two parallel diabatic levels, which could invoke a subtle treatment of the WKB analysis. Nevertheless, we think that our present result must be taken as a tentative conclusion concerning the visibility of new Stokes curves because our analysis has been made in a rather heuristic manner, and therefore should be pursued as a future investigation.

Finally, we would like to make some remarks on a multistate nonadiabatic transition problem in view of the WKB analysis. Our main concern throughout this paper was to explore how essentially different is the multistate nonadiabatic transition model from the two-state model. In this regard, there are two new aspects to be especially emphasized. Virtual turning points and new Stokes curves are obviously new building blocks, which are absent in the WKB analysis in the two-state models, and are predicted in a highly nontrivial manner. We may say for this reason that these are definitely specific in multistate models and their roles should be studied more systematically and closely.

One more aspect we should not overlook is that the form of the WKB solution derived in the course of the analysis properly incorporate the phase gained in the time evolution. As a consequence, it became possible to have an explicit expression for the connection matrix and the S matrix when the reality condition is satisfied. This in turn might lead us to explore under which conditions the independent crossing approximation works, which has been often asked in the studies of the multistate nonadiabatic transition problem.

ACKNOWLEDGMENTS

The authors are grateful to Takashi Aoki, Naofumi Honda, Takahiro Kawai, Tatsuya Koike, Shinji Sasaki, and Yoshitsugu Takei for their valuable comments and stimulating discussions on the exact WKB method. This work has been supported by JSPS KAKENHI Grants No. 15H03701 and No. 17K05583.

APPENDIX A: REDUCTION TO THE LANDAU-ZENER MODEL AND THE CONNECTION FORMULA FOR THE WKB SOLUTION

In this Appendix we show the derivation of the connection formula (14) for the WKB solution (10). The following derivation is fully based on that presented in [37,51], but some more details, especially on a proper choice of local WKB solutions, which is in fact crucial to proceed with the analysis, will not be given below. We also do not touch on the Borel sum and the associated summability, although there has been substantial progress around this issue.

As is expected, the connection around each turning point at $t = t_{jk}^{[n]}$ can be reduced locally to that in the case with a double turning point, that is, the Landau-Zener model for the two states:

$$i\frac{d}{dz}\begin{pmatrix}\varphi_1\\ \varphi_2\end{pmatrix} = \eta\left[\begin{pmatrix}-z & 0\\ 0 & z\end{pmatrix} + \eta^{-1/2}\begin{pmatrix}0 & \mu\\ \nu & 0\end{pmatrix}\right]\begin{pmatrix}\varphi_1\\ \varphi_2\end{pmatrix}, \tag{A1}$$

with some two constants μ and ν.

The reduction of the original model (3) to the Landau-Zener model (A1) is achieved by taking the following steps. Let $t = \tau$ be a turning point of (3) with type (j,k), that is, $\rho_j(\tau) = \rho_k(\tau) \neq \rho_l(\tau)$ holds for a permutation of $\{j,k,l\}$ of $\{1,2,3\}$. We first transform Eq. (3) to a coupled equations with a block-diagonal form

$$i\frac{d}{dt}\varphi = \eta K(t,\eta)\varphi, \tag{A2}$$

where

$$K(t,\eta) = \begin{pmatrix}\rho_j(t) & 0 & 0\\ 0 & \rho_k(t) & 0\\ 0 & 0 & \rho_l(t)\end{pmatrix} + \eta^{-1/2}\left(\begin{array}{cc|c} & & 0\\ & K^{(j,k)}(t,\eta) & 0\\ & & \\ \hline 0 & 0 & K^{(l)}(t,\eta)\end{array}\right) \tag{A3}$$

via a formal transformation

$$\psi = S(t,\eta)\varphi = [\mathrm{Id} + \eta^{-1/3}S_{1/2}(t) + \eta^{-1}S_(t) + \cdots]\varphi.$$

Here $K^{(j,k)}(t,\eta)$ is a formal power series of $\eta^{-1/2}$ with 2×2 matrix coefficients and $K^{(l)}(t,\eta)$ is a scalar formal power series. As a result of this block diagonalization, the connection problem near an ordinary turning point of type (j,k) is reduced to that for a 2×2 system

$$i\frac{d}{dt}\Psi = \eta\left[\begin{pmatrix}\rho_j(t) & 0\\ 0 & \rho_k(t)\end{pmatrix} + \eta^{-1/2}K^{(j,k)}(t,\eta)\right]\Psi. \tag{A4}$$

This system is further transformed to the Landau-Zener model (A1) with $\mu = \mu_0 + \eta^{-1/2}\mu_{1/2} + \cdots$ and $\nu = \nu_0 + \eta^{-1/2}\nu_{1/2} + \cdots$ by a formal transformation

$$\psi = \exp\Big(\frac{\eta}{2i}\int^t (\rho_j(t) + \rho_k(t))dt\Big)T(t,\eta)\varphi,$$

with

$$T(t,\eta) = \sum_{n=0}^{\infty}\eta^{-n/2}T_{n/2}(t),$$

and a change of variables

$$z = \Big(\int_\tau^t [\rho_k(t) - \rho_j(t)]dt\Big)^{1/2}.$$

Here $T_{n/2}(t)$ $(n = 0, 1, 2\ldots)$ is a 2×2 matrix with holomorphic matrix entries at $t = \tau$ with $\det T_0(\tau) \neq 0$. The constants $(\mu_{n/2}, \nu_{n/2})$ are uniquely determined by the original system (3).

It is easy to see that (A1) is equivalent to the Weber equation, and a fundamental system of solutions can be expressed as

$$\begin{aligned}\varphi^{(+)} &= \eta^{-1/2}\left\{\begin{pmatrix}1\\ \frac{-\eta^{-1/2}\nu}{2z}\end{pmatrix} + O(\eta^{-1/2})\right\}e^{i\eta z^2/2}e^{i\mu\nu/2}\\ &\quad\times[1 + O(\eta^{-1/2})],\\ \varphi^{(-)} &= \eta^{-1/2}\left\{\begin{pmatrix}\frac{\eta^{-1/2}\mu}{2z}\\ 1\end{pmatrix} + O(\eta^{-1/2})\right\}e^{i\eta z^2/2}e^{i\mu\nu/2}\\ &\quad\times[1 + O(\eta^{-1/2})].\end{aligned} \tag{A5}$$

The Stokes phenomenon for the Weber equation was studied for example in a literature [60], and a more comprehensive analysis based on the exact WKB analysis was made in Ref. [61] by introducing a properly normalized WKB solution. This provides connection formulas around a double turning point from which four Stokes curves emanate. When applying the connection formulas thus obtained to form the solutions (A5), we can establish the analytic continuation of the WKB solution (precisely the Borel summed WKB solution) across a Stokes curve $\{z\in\mathbb{C}\,|\,\arg z = \pi/4\}$ in the anticlockwise direction as

$$\begin{aligned}&\varphi^{(+)} \longmapsto \varphi^{(+)},\\ &\varphi^{(-)} \longmapsto \varphi^{(-)} + (2\eta)^{i\mu\nu/2}\frac{\mu\sqrt{\pi}}{\Gamma(i\mu\nu/2+1)}e^{\pi(1+\mu\nu)/4}\varphi^{(+)},\end{aligned} \tag{A6}$$

and when crossing a Stokes curve $\{z\in\mathbb{C}\,|\,\arg z = 3\pi/4\}$ anticlockwise, we have

$$\begin{aligned}&\varphi^{(+)} \longmapsto \varphi^{(+)} + (2\eta)^{-i\mu\nu/2}\frac{\nu\sqrt{\pi}}{\Gamma(-i\mu\nu/2+1)}e^{3\pi(i-\mu\nu)/4}\varphi^{(-)},\\ &\varphi^{(-)} \longmapsto \varphi^{(-)}.\end{aligned} \tag{A7}$$

Combined with these, the following connection formulas hold when we cross the two Stokes curves $\{z\in\mathbb{C}\,|\,\arg z = \pi/4\}$

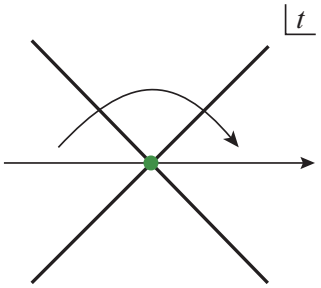

FIG. 18. Analytic continuation of $(\varphi^{(+)}, \varphi^{(-)})$ across the Stokes curves $\{z\in\mathbb{C}\,|\,\arg z = \pi/4\}$ and $\{z\in\mathbb{C}\,|\,\arg z = 3\pi/4\}$.

and $\{z \in \mathbb{C} \mid \arg z = 3\pi/4\}$ from the left to the right (i.e., clockwise) in the upper half z plane (see Fig. 18):

$$\varphi^{(+)} \longmapsto e^{-\pi\mu\nu}\varphi^{(+)} - (2\eta)^{-i\mu\nu/2}\frac{\nu\sqrt{\pi}}{\Gamma(-i\mu\nu/2+1)}e^{3\pi(i-\mu\nu)/4}\varphi^{(-)}, \tag{A8}$$

$$\varphi^{(-)} \longmapsto \varphi^{(-)} - (2\eta)^{i\mu\nu/2}\frac{\mu\sqrt{\pi}}{\Gamma(i\mu\nu/2+1)}e^{\pi(1+\mu\nu)/4}\varphi^{(+)}. \tag{A9}$$

We now plug such a connection formula for a fundamental system of solutions (A5) of the Landau-Zener model into the original model (3). For that purpose we introduce local WKB solutions of the form, which are equivalent to (19) and (20) in the main text,

$$\begin{aligned}\psi_0^{(j)} &= \eta^{-\frac{1}{2}}\exp\left\{\frac{\eta}{i}\int_{t_{jk}}^{t}\rho_j(t')dt' + \frac{1}{i}\int_{t_{jk}}^{t}\left[|c_{jk}|^2\left(\frac{1}{\rho_j-\rho_k}+\frac{1}{\lambda_{jk}(t-t_{jk})}\right)+\frac{|c_{jl}|^2}{\rho_j-\rho_l}\right]dt'\right\}\\ &\quad\times\left(\frac{\lambda_{jk}(t-t_{jk})^2}{2}\right)^{\frac{\kappa_{jk}}{2}}\left(e^{(j)}+O(\eta^{-1/2})\right),\end{aligned} \tag{A10}$$

$$\begin{aligned}\psi_0^{(k)} &= \eta^{-1/2}\exp\left\{\frac{\eta}{i}\int_{t_{jk}}^{t}\rho_j(t')dt' + \frac{1}{i}\int_{t_{jk}}^{t}\left[-|c_{jk}|^2\left(\frac{1}{\rho_j-\rho_k}+\frac{1}{\lambda_{jk}(t-t_{jk})}\right)+\frac{|c_{kl}|^2}{\rho_k-\rho_l}\right]dt'\right\}\\ &\quad\times\left(\frac{\lambda_{jk}(t-t_{jk})^2}{2}\right)^{-\frac{\kappa_{jk}}{2}}\left(e^{(k)}+O(\eta^{-1/2})\right).\end{aligned} \tag{A11}$$

It can be verified by a straightforward computation that the following relations hold between the above local WKB solutions $\psi_0^{(j)}$ and $\psi_0^{(k)}$ and a fundamental system of solutions $\varphi^{(+)}$ and $\varphi^{(-)}$:

$$\begin{aligned}\psi_0^{(j)} &= S(t,\eta)\exp\left(\frac{\eta}{2i}\int^t[\rho_j(t)+\rho_k(t)]dt\right)\\ &\quad\times\begin{pmatrix}T(z,\eta)\varphi^{(+)}\\ 0\end{pmatrix}\Bigg|_{z=z(t)}[1+O(\eta^{-1})],\\ \psi_0^{(k)} &= S(t,\eta)\exp\left(\frac{\eta}{2i}\int^t[\rho_j(t)+\rho_k(t)]dt\right)\\ &= \begin{pmatrix}T(z,\eta)\varphi^{(-)}\\ 0\end{pmatrix}\Bigg|_{z=z(t)}[1+O(\eta^{-1})].\end{aligned}$$

Thus the connection formulas (A10) and (A11) for $\varphi^{(+)}$ and $\varphi^{(-)}$ lead to those for $\psi_0^{(j)}$ and $\psi_0^{(k)}$:

$$\begin{aligned}\psi_0^{(j)} &\longmapsto e^{2i\pi\kappa_{jk}}[1+O(\eta^{-1/2})]\psi_0^{(j)}\\ &\quad- (2\eta)^{-\kappa_{jk}}\sqrt{\frac{2\pi}{\lambda_{jk}}}\frac{\overline{c_{jk}}}{\Gamma(1-\kappa_{jk})}e^{3i\pi(1+2\kappa_{jk})/4}\\ &\quad\times[1+O(\eta^{-1/2})]\psi_0^{(k)},\end{aligned} \tag{A12}$$

$$\begin{aligned}\psi_0^{(k)} &\longmapsto [1+O(\eta^{-1/2})]\psi_0^{(k)}\\ &\quad- (2\eta)^{-\kappa_{jk}}\sqrt{\frac{2\pi}{\lambda_{jk}}}\frac{c_{jk}}{\Gamma(1+\kappa_{jk})}e^{i\pi(1-2\kappa_{jk})/4}\\ &\quad\times[1+O(\eta^{-1/2})]\psi_0^{(j)}.\end{aligned} \tag{A13}$$

Combining the above connection formulas with the relations (18), we finally obtain the connection formulas (14) for WKB solutions $\psi^{(j)}$ $(j=1,2,3)$.

APPENDIX B: RATIO BETWEEN GLOBAL AND LOCAL WKB SOLUTIONS

In this Appendix we provide an explicit form of the ratio β_{jk} given by (17) (we here drop a superscript $[n]$ in (17) for notational simplicity). We here consider the ratio at a turning point $t = t_{jk,m}$, which is a turning point of type (j,k) and the index m has to be introduced because the number of turning points with a fixed type (j,k) is more than one when diabatic energy functions $\rho_1(t)$, $\rho_2(t)$, and $\rho_3(t)$ are nonlinear. We assume

$$\rho_j(t) - \rho_k(t) = a\prod_{m=1}^{p}(t-t_{jk,m}), \tag{B1}$$

where $p(t)$ denotes the highest degree of the polynomial $\rho_j(t)-\rho_k(t)$ and a the corresponding coefficient. In a similar way, let q and r be the highest degrees of the polynomials $\rho_k(t)-\rho_l(t)$ and $\rho_l(t)-\rho_j(t)$, respectively. Since the equation $[\rho_1(t)-\rho_2(t)][\rho_2(t)-\rho_3(t)][\rho_3(t)-\rho_1(t)] = 0$ has simple zeros [see the reality assumption (7)], a straightforward calculation with the help of the residue theorem leads to

$$\frac{1}{\rho_j-\rho_k} = -\sum_{m=1}^{p}\frac{1}{\lambda_{jk,m}(t-t_{jk,m})}, \tag{B2}$$

where

$$\lambda_{jk,m} = \frac{d}{dt}(\rho_j-\rho_k)\Big|_{t=t_{jk,m}}. \tag{B3}$$

A global WKB solution (10) is then rewritten as

$$\begin{aligned}\psi_j(t) &= \eta^{-1/2}\exp\left(\frac{\eta}{i}\int_{t_0}^{t}\rho_j(t')dt'\right)\prod_{m=1}^{p}(t-t_{jk,m})^{\kappa_{jk,m}}\\ &\quad\times\prod_{m'=1}^{q}(t-t_{jl,m'})^{\kappa_{jl,m'}}\left(e^{(j)}+O(\eta^{-1/2})\right),\end{aligned} \tag{B4}$$

where

$$\kappa_{jk,m} = \frac{i|c_{ji}|^2}{\lambda_{jk,m}}, \tag{B5}$$

and the base point t_0 is taken to be arbitrary.

In a similar vein we can rewrite local WKB solutions around a turning point at $t = t_{jk,1}$ as

$$\begin{aligned}
\psi_0^{(j)} &= \eta^{-1/2}\exp\left\{\frac{\eta}{i}\int_{t_{jk}}^{t}\rho_j(t')dt'\right. \\
&\quad \left. + \frac{1}{i}\int_{t_{jk,1}}^{t}\left[-|c_{jk}|^2\left(\sum_{m=2}^{p}\frac{1}{\lambda_{jk,m}(t-t_{jk,m})}\right)\right.\right. \\
&\quad \left.\left. + \frac{|c_{jl}|^2}{\rho_j-\rho_l}\right]dt'\right\}\left(\frac{\lambda_{jk,1}(t-t_{jk,1})^2}{2}\right)^{\frac{\kappa_{jk,1}}{2}} \\
&\quad \times\left(e^{(j)}+O(\eta^{-1/2})\right) \\
&= \eta^{-1/2}\exp\left(\frac{\eta}{i}\int_{t_{jk,1}}^{t}\rho_j(t')dt'\right)\prod_{m=1}^{p}(t-t_{jk,m})^{\kappa_{jk,m}} \\
&\quad \times\prod_{m=2}^{p}(t_{jk,1}-t_{jk,m})^{-\kappa_{jk,m}}\prod_{m=1}^{q}(t-t_{jl,m})^{\kappa_{jl,m}} \\
&\quad \times\prod_{m=1}^{q}(t_{jk,1}-t_{jl,m})^{-\kappa_{jl,m}}\left(\frac{\lambda_{jk,1}}{2}\right)^{\frac{\kappa_{jk,1}}{2}} \\
&\quad \times\left(e^{(j)}+O(\eta^{-1/2})\right),
\end{aligned} \tag{B6}$$

$$\begin{aligned}
\psi_0^{(k)} &= \eta^{-1/2}\exp\left\{\frac{\eta}{i}\int_{t_{jk}}^{t}\rho_j(t')dt'\right. \\
&\quad \left. + \frac{1}{i}\int_{t_{jk,1}}^{t}\left[|c_{jk}|^2\left(\sum_{m=2}^{p}\frac{1}{\lambda_{jk,m}(t-t_{jk,m})}\right)\right.\right. \\
&\quad \left.\left. + \frac{|c_{kl}|^2}{\rho_k-\rho_l}\right]dt'\right\}\left(\frac{\lambda_{jk,1}(t-t_{jk,1})^2}{2}\right)^{\frac{\kappa_{jk,1}}{2}} \\
&\quad \times\left(e^{(j)}+O(\eta^{-1/2})\right), \\
&= \eta^{-1/2}\exp\left(\frac{\eta}{i}\int_{t_{jk,1}}^{t}\rho_j(t')dt'\right)\prod_{m=1}^{p}(t-t_{jk,m})^{-\kappa_{jk,m}} \\
&\quad \times\prod_{m=2}^{p}(t_{jk,1}-t_{jk,m})^{\kappa_{jk,m}}\prod_{m=1}^{r}(t-t_{kl,m})^{\kappa_{kl,m}} \\
&\quad \times\prod_{m=1}^{r}(t_{jk,1}-t_{kl,m})^{-\kappa_{kl,m}}\left(\frac{\lambda_{jk,1}}{2}\right)^{-\frac{\kappa_{jk,1}}{2}} \\
&\quad \times\left(e^{(k)}+O(\eta^{-1/2})\right).
\end{aligned} \tag{B7}$$

Recalling the relations

$$\psi_0^{(j)} = \gamma_j\psi^{(j)}, \quad \psi_0^{(k)} = \gamma_k\psi^{(k)}, \tag{B8}$$

and

$$\beta_{jk} = \gamma_j/\gamma_k, \tag{B9}$$

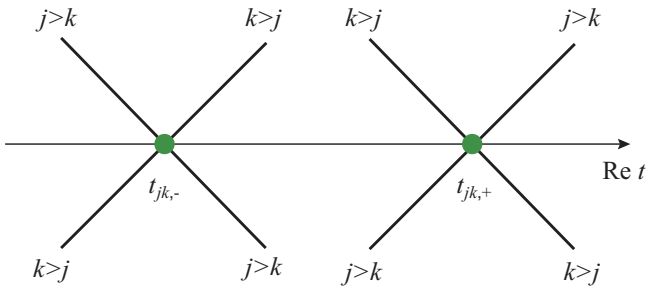

FIG. 19. The dominance relation on Stokes curves when the turning points $t = t_{ij,-}$ and $t = t_{ij,+}$ are both located on the real axis.

we obtain an explicit expression

$$\begin{aligned}
\beta_{jk} &= \exp\left(\frac{\eta}{i}\int_{t_{jk,1}}^{t_0}[\rho_j(t')-\rho_k(t')]dt'\right) \\
&\quad \times\prod_{m=2}^{p}(t_{jk,1}-t_{jk,m})^{-2\kappa_{jk,m}}\prod_{m=1}^{q}(t_{jk,1}-t_{jl,m})^{-\kappa_{jl,m}} \\
&\quad \times\prod_{m=1}^{q}(t_{jk,1}-t_{kl,r})^{\kappa_{kl,m}}\left(\frac{\lambda_{jk,1}}{2}\right)^{\kappa_{jk,1}}.
\end{aligned}$$

APPENDIX C: STOKES COEFFICIENTS ON RESOLVED STOKES CURVES

In this Appendix we show how Stokes coefficients behave when we resolve a degenerated Stokes curve connecting a complex conjugate pair of turning points.

As illustrated in Fig. 12, a degenerated Stokes curve is resolved by adding a small imaginary perturbation to a diabatic energy state. In order to see the behavior of the corresponding Stokes coefficients, suppose that diabatic energy levels forming a pair of complex conjugate turning points take the form as

$$\begin{aligned}
\rho_j(t)-\rho_k(t) &= at^2+bt+c+i\varepsilon \\
&= a(t-t_{jk,+})(t-t_{jk,-}),
\end{aligned} \tag{C1}$$

$$\rho_k(t)-\rho_l(t) = \prod_{m=1}^{q}(t-t_{kl,m}), \tag{C2}$$

$$\rho_l(t)-\rho_j(t) = \prod_{m=1}^{r}(t-t_{lj,m}), \tag{C3}$$

where $a > 0$, b and c are real constants. The parameter ε will be used to resolve the degeneracy. We may multiply the right-hand side by a certain polynomial to yield a more general form as far as the local topology of the Stokes geometry is kept. We may also set the top order coefficients for $\rho_k(t)-\rho_l(t)$ and $\rho_l(t)-\rho_j(t)$ to be unity without loss of generality.

When the turning points $t = t_{ij,\pm}$ are both real, one can easily check that the dominance relation on each Stokes curve is given as Fig. 19. This can be confirmed, for example, in the case of a Stokes curve emanating from a turning point

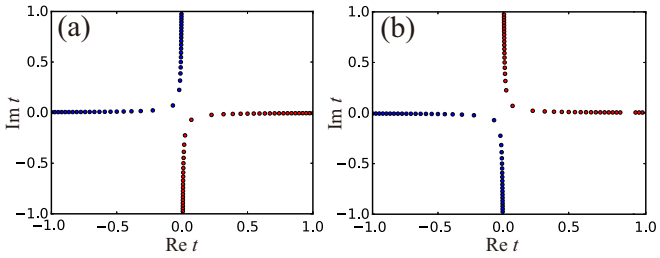

FIG. 20. The behavior of turning points on the complex t plane as the parameter c is changed from -1 to $+1$, keeping other parameters $a = 1$, $b = 0$ being fixed. The magnitude of perturbation is respectively given as (a) $\varepsilon = +0.001$ and (b) $\varepsilon = -0.001$. The blue and red dots, respectively, denote the position of turning points $t = t_{ij,-}$ and $t = t_{ij,+}$.

$t = t_{ij,-}$ and heading in the $3\pi/4$ direction, by calculating

$$\mathrm{Re}\left[\frac{1}{i}\int_{t_{jk,-}}^{t} Q(t')dt'\right] = \frac{\sqrt{b^2-4ac}}{2}|t - t_{ij,-}|^2 > 0 \quad \text{(C4)}$$

for $|t - t_{ij,-}| \ll 1$. Here $Q(t) := \rho_j(t) - \rho_k(t)$. The dominance relation on other Stokes curves is similarly determined.

With increase in c, the two real turning points $t = t_{ij,\pm}$ come close to each other and form a complex conjugate pair. Before the degeneracy, Stokes curves emanating from each turning point $t = t_{ij,\pm}$ always tend to infinity, meaning that only a single turning point exists on each Stokes curve. On the other hand, after the collision of the two turning points $t = t_{ij,\pm}$, giving rise to the degeneracy, a complex conjugate turning points $t = t_{ij,\pm}$ are connected by a single Stokes curve as depicted in Fig. 12. As demonstrated in Fig. 20, the degeneracy is resolved by adding a small imaginary perturbation to $\rho_j(t) - \rho_k(t)$, and a degenerated Stokes curve connecting the two turning points is split into two separated Stokes curves as illustrated in Fig. 21. The resulting configuration of turning points and the associated Stokes curves depend on the sign of ε. Note that in Fig. 21 a turning point $t = t_{ij,-}$ designates the one which was originally located on the left side, and a turning point $t = t_{ij,+}$ the one coming from the right-hand side (see Fig. 19). Note that the direction of Stokes curves is given by the formula

$$\arg(t-\tau) = \left[-\frac{3\pi}{4}, -\frac{\pi}{4}, \frac{\pi}{4}, \frac{3\pi}{4}\right] - \frac{1}{2}\arg Q'(\tau), \quad \text{(C5)}$$

where τ denotes a turning point.

We now calculate Stokes coefficients $\alpha_{jk,\pm}$ and $\alpha_{kj,\pm}$. First, it is easy to show that

$$\lim_{\varepsilon\to+0} t_{jk,\mp} = \lim_{\varepsilon\to-0} t_{jk,\pm} \quad \text{(C6)}$$

holds. To calculate the ratio $\beta_{jk,\pm}$ (or $\beta_{kj,\pm}$), which connects global and local WKB solutions, we prepare some relations. For arbitrary ε we can show that

$$\lambda_{jk,-} := \frac{d}{dt}(\rho_k - \rho_j)\bigg|_{t=t_{jk,-}} = a(t_{jk,+} - t_{jk,-}),$$

$$\lambda_{kj,+} := \frac{d}{dt}(\rho_j - \rho_k)\bigg|_{t=t_{jk,+}} = a(t_{jk,+} - t_{jk,-}),$$

and

$$\lambda_{jk,-} = \lambda_{kj,+} \quad \text{(C7)}$$

hold, and also it is easy to check

$$\lim_{\varepsilon\to-0} \lambda_{jk,-} = -\lim_{\varepsilon\to+0} \lambda_{jk,-}. \quad \text{(C8)}$$

These relations immediately lead to

$$\kappa_{jk,-} = \kappa_{kj,+}, \quad \text{(C9)}$$

$$\lim_{\varepsilon\to-0} \kappa_{jk,-} = -\lim_{\varepsilon\to+0} \kappa_{jk,-}, \quad \text{(C10)}$$

where

$$\kappa_{ji,\pm} := \frac{i|c_{jk}|^2}{\lambda_{jk,\pm}}. \quad \text{(C11)}$$

Next we examine the direction of Stokes curves emanating from each turning point located in the complex plane. For $\varepsilon < 0$, recalling that $\mathrm{Im}(t_{jk,+}) > \mathrm{Im}(t_{jk,-})$ we have

$$\arg\left\{\frac{d}{dt}(\rho_k - \rho_j)\bigg|_{t=t_{jk,-}}\right\} = \arg\left\{\frac{d}{dt}(\rho_j - \rho_k)\bigg|_{t=t_{jk,+}}\right\}$$
$$= \arg\{a(t_{jk,+} - t_{jk,-})\} = \frac{\pi}{2}.$$

Hence the direction of Stokes curves is respectively given as

$$\arg(t - t_{jk,\pm}) = \left[-\pi, -\frac{\pi}{2}, 0, \frac{\pi}{2}\right] \quad (\varepsilon \to -0). \quad \text{(C12)}$$

Similarly, for $\varepsilon > 0$, since $\mathrm{Im}(t_{jk,-}) > \mathrm{Im}(t_{jk,+})$ holds, we get the direction of Stokes curves as

$$\arg(t - t_{jk,\pm}) = \left[-\frac{\pi}{2}, 0, \frac{\pi}{2}, \pi\right] \quad (\varepsilon \to +0). \quad \text{(C13)}$$

Then we can specify the direction of Stokes curves which are revolved by adding a perturbation. As actually shown in Fig. 21, for $\varepsilon \to +0$, resolved Stokes curves are the ones satisfying $\arg(t - t_{jk,+}) = \pi/2$ and $\arg(t - t_{jk,-}) = -\pi/2$, whereas in the case of $\varepsilon \to -0$ we have $\arg(t - t_{jk,+}) = -\pi/2$ and $\arg(t - t_{jk,-}) = \pi/2$ as resolved Stokes curves. From the relations (C5), (C12), and (C13) we notice that

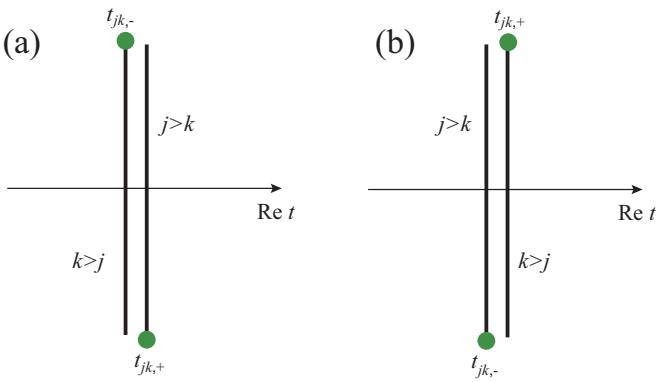

FIG. 21. Two resolved patterns of the local Stokes geometry after the degeneracy. Configuration (a) is realized for $\varepsilon > 0$, while the pattern (b) appears for $\varepsilon < 0$. The dominance relation on Stokes curves is inserted in the figures. The turning points $t = t_{ij,\pm}$ nearly form a complex conjugate pair as far as $|\varepsilon| \ll 1$ holds.

each Stokes curve respectively originates from Stokes curves with $\arg(t-t_{jk,+})=-\pi/4$, $\arg(t-t_{jk,-})=3\pi/4$, $\arg(t-t_{jk,+})=\pi/4$, and $\arg(t-t_{jk,-})=-3\pi/4$, when turning points $t_{jk,\pm}$ are located on the real axis.

On the basis of these these observations, we can calculate the ratio $\beta_{jk,\pm}$ (or $\beta_{kj,\pm}$) by applying the recipe presented in Appendix B. First we consider the case where the dominance relation $j>k$ holds. This is concerned with the right Stokes curve in Fig. 21(a) and the left Stokes curve in Fig. 21(b).

For the Stokes curve satisfying $\arg(t-t_{jk,+})=\pi/2$ in the limit of $\varepsilon\to+0$, we obtain

$$\begin{aligned}\alpha_{kj,+} &= (2\eta)^{\kappa_{kj,+}}\sqrt{\frac{2\pi}{\lambda_{kj,+}}}\frac{c_{kj}}{\Gamma(1+\kappa_{kj,+})}\\ &\quad\times e^{-\frac{1}{2}i\pi\kappa_{kj,+}+\frac{1}{4}i\pi}(\beta_{kj,+}),\\ \beta_{kj,+} &= \exp\left[\frac{\eta}{i}\int_{t_{jk,+}}^{t_0}(\rho_k-\rho_j)dt\right]\\ &\quad\times(t_{jk,+}-t_{jk,-})^{-2\kappa_{kj,-}}\prod_{m=1}^{r}(t_{jk,+}-t_{kl,m})^{-\kappa_{kl,m}}\\ &\quad\times\prod_{m=1}^{q}(t_{jk,+}-t_{jl,m})^{\kappa_{jl,m}}\left(\frac{\lambda_{kj,+}}{2}\right)^{\kappa_{kj,+}}.\end{aligned}$$

Similarly, for the Stokes curve satisfying $\arg(t-t_{jk,-})=\pi/2$ in the limit of $\varepsilon\to-0$, we obtain

$$\begin{aligned}\alpha_{jk,-} &= (2\eta)^{-\kappa_{jk,-}}\sqrt{\frac{2\pi}{\lambda_{jk,-}}}\frac{\overline{c_{jk}}}{\Gamma(1-\kappa_{jk,-})}\\ &\quad\times e^{\frac{3}{2}i\pi\kappa_{jk,-}+\frac{3}{4}i\pi}(\beta_{jk,-})^{-1},\\ \beta_{jk,-} &= \exp\left[\frac{\eta}{i}\int_{t_{jk,-}}^{t_0}(\rho_j-\rho_k)dt\right]\\ &\quad\times(t_{jk,-}-t_{jk,+})^{-2\kappa_{jk,+}}\prod_{m=1}^{q}(t_{jk,-}-t_{jl,m})^{-\kappa_{jl,m}}\\ &\quad\times\prod_{m=1}^{r}(t_{jk,-}-t_{kl,m})^{\kappa_{kl,m}}\left(\frac{\lambda_{jk,-}}{2}\right)^{\kappa_{jk,-}}.\end{aligned}$$

From the relations (C6), (C8), and (C10) we find

$$\lim_{\varepsilon\to+0}\beta_{kj,+}e^{i\pi\kappa_{kj,+}}=\lim_{\varepsilon\to-0}(\beta_{jk,-})^{-1},\tag{C14}$$

which leads to

$$\lim_{\varepsilon\to+0}\alpha_{kj,+}=\lim_{\varepsilon\to-0}\alpha_{jk,-}.\tag{C15}$$

The final relation tells us that the Stokes coefficients with the same dominance relation $j>k$ coincide with each other as $\varepsilon\to\pm0$.

In the same way, for the Stokes curves on which the dominance relation $k>j$ holds, we have the following explicit formulas for the Stokes coefficient. For the Stokes curve

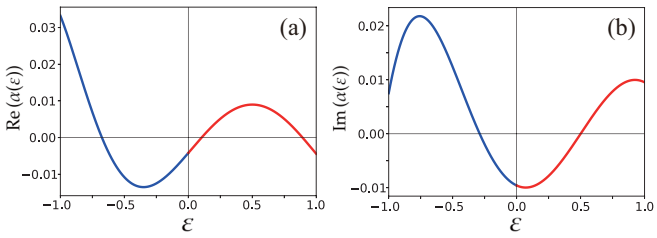

FIG. 22. (a) The real and (b) imaginary part of the Stokes coefficient for the Stokes curve with the dominance relation $1>3$ is plotted. Blue and red curves represent the Stokes coefficients for $\varepsilon<0$ and $\varepsilon>0$, respectively. The set of parameters are the same as in that used for Figs. 11(c) and 11(d).

satisfying $\arg(t-t_{jk,-})=-\pi/2$ in the limit of $\varepsilon\to+0$, we have

$$\begin{aligned}\alpha_{jk,-} &= (2\eta)^{\kappa_{jk,-}}\sqrt{\frac{2\pi}{\lambda_{jk,-}}}\frac{c_{jk}}{\Gamma(1+\kappa_{jk,-})}\\ &\quad\times e^{\frac{3}{2}i\pi\kappa_{jk,-}-\frac{3}{4}i\pi}(\beta_{jk,-}),\\ \beta_{jk,-} &= \exp\left[\frac{\eta}{i}\int_{t_{jk,-}}^{t_0}(\rho_j-\rho_k)dt\right]\\ &\quad\times(t_{jk,-}-t_{jk,+})^{-2\kappa_{jk,+}}\prod_{m=1}^{q}(t_{jk,-}-t_{jl,m})^{-\kappa_{jl,m}}\\ &\quad\times\prod_{m=1}^{r}(t_{jk,-}-t_{kl,m})^{\kappa_{kl,m}}\left(\frac{\lambda_{jk,-}}{2}\right)^{\kappa_{jk,-}},\end{aligned}$$

and for the Stokes curve given by $\arg(t-t_{jk,+})=-\pi/2$ in the limit of $\varepsilon\to-0$ we obtain

$$\begin{aligned}\alpha_{kj,+} &= (2\eta)^{-\kappa_{kj,+}}\sqrt{\frac{2\pi}{\lambda_{kj,+}}}\frac{\overline{c_{kj}}}{\Gamma(1-\kappa_{kj,+})}\\ &\quad\times e^{-\frac{1}{2}i\pi\kappa_{kj,+}-\frac{1}{4}i\pi}(\beta_{kj,+})^{-1},\\ \beta_{kj,+} &= \exp\left[\frac{\eta}{i}\int_{t_{jk,+}}^{t_0}(\rho_k-\rho_j)dt\right]\\ &\quad\times(t_{jk,+}-t_{jk,-})^{-2\kappa_{kj,-}}\prod_{m=1}^{r}(t_{jk,+}-t_{kl,m})^{-\kappa_{kl,m}}\\ &\quad\times\prod_{m=1}^{q}(t_{jk,+}-t_{jl,m})^{\kappa_{jl,m}}\left(\frac{\lambda_{kj,+}}{2}\right)^{\kappa_{kj,+}}.\end{aligned}$$

Again from the relations (C6), (C8), and (C10), we can show

$$\lim_{\varepsilon\to+0}\beta_{jk,-}e^{i\pi\kappa_{jk,-}}=\lim_{\varepsilon\to-0}(\beta_{kj,+})^{-1},\tag{C16}$$

which leads to

$$\lim_{\varepsilon\to+0}\alpha_{jk,-}=\lim_{\varepsilon\to-0}\alpha_{kj,+}.\tag{C17}$$

In this way, irrespective of the sign of the perturbation ε, the Stokes coefficients on the Stokes curves with the same dominance relation tend to the same limiting value as $\varepsilon\to\pm0$. We plot in Fig. 22 the Stokes coefficient for a Stokes curve with the dominance relation $1>3$ (see Fig. 12).

[1] H. Nakamura, *Nonadiabatic Transition: Concepts, Basic Theories and Applications* (World Scientific, Singapore, 2012).
[2] L. D. Landau, *Collected Papers of L.D. Landau*, edited by D. Ter Haar (Elsevier, Amsterdam, 1965), pp. 63–66.
[3] C. Zener, Proc. R. Soc. London Ser. A **137**, 696 (1932).
[4] E. Majorana, Nuovo Cimento **9**, 43 (1932).
[5] *E.C.G. Stueckelberg, An Unconventional Figure of Twentieth Century Physics*, edited by J. Lacki, H. Ruegg, and G. Wanders (Birkhuser Basel, 2009), pp. 117–171.
[6] J. Heading, *An Introduction to Phase-Integral Methods* (Dover Books on Mathematics, New York, 1961).
[7] M. V. Berry and K. E. Mount, Rep. Prog. Phys. **35**, 315 (1972).
[8] V. P. Maslov and M. V. Fedoriuk, *Semi-Classical Approximation in Quantum Mechanics, Mathematical Physics and Applied Mathematics* (Springer, New York, 1981); Yu. N. Demkov and V. I. Osherov, Zh. Éksp. Teor. Fiz. **53**, 1589 (1967) [Sov. Phys. JETP **26**, 916 (1968)].
[9] V. I. Osherov, Zh. Éksp. Teor. Fiz. **49**, 1157 (1965) [Sov. Phys. JETP **22**, 804 (1966)].
[10] Yu. N. Demkov, Dokl. Akad. Nauk SSSR **166**, 1076 (1966) [Sov. Phys. Dokl. **11**, 138 (1966)].
[11] Y. N. Demkov and V. N. Ostrovsky, J. Phys. B **28**, 403 (1995).
[12] T. Usuki, Phys. Rev. B **56**, 13360 (1997).
[13] V. N. Ostrovsky and H. Nakamura, Phys. Rev. A **58**, 4293 (1998).
[14] V. L. Pokrovsky and N. A. Sinitsyn, Phys. Rev. B **65**, 153105 (2002).
[15] N. A. Sinitsyn, J. Phys. A **37**, 10691 (2004).
[16] A. V. Shytov, Phys. Rev. A **70**, 052708 (2004).
[17] M. V. Volkov and V. N. Ostrovsky, Phys. Rev. A **75**, 022105 (2007).
[18] N. A. Sinitsyn and F. Li, Phys. Rev. A **93**, 063859 (2016).
[19] N. A. Sinitsyn, J. Phys. A **48**, 195305 (2015).
[20] N. A. Sinitsyn, Phys. Rev. B **92**, 205431 (2015).
[21] A. Patra and E. A. Yuzbashyan, J. Phys. A **48**, 245303 (2015).
[22] N. A. Sinitsyn, J. Lin, and V. Y. Chernyak, Phys. Rev. A **95**, 012140 (2017).
[23] N. A. Sinitsyn and V. Y. Chernyak, J. Phys. A **50**, 255203 (2017).
[24] C. E. Carroll and F. T. Hioe, J. Phys. A **19**, 1151 (1986).
[25] C. E. Carroll and F. T. Hioe, J. Opt. Soc. Am. B **2**, 1355 (1985); J. Phys. A **19**, 2061 (1986).
[26] V. N. Ostrovsky and H. Nakamura, J. Phys. A **30**, 6939 (1997).
[27] Y. N. Demkov and V. N. Ostrovsky, Phys. Rev. A **61**, 032705 (2000).
[28] Y. N. Demkov and V. N. Ostrovsky, J. Phys. B **34**, 2419 (2001).
[29] V. N. Ostrovsky, Phys. Rev. A **68**, 012710 (2003).
[30] N. A. Sinitsyn, Phys. Rev. A **90**, 062509 (2014).
[31] J. Lin and N. A. Sinitsyn, J. Phys. A: Math. Theor. **47**, 015301 (2014).
[32] S. Brundobler and V. Elser, J. Phys. A: Math. Gen. **26**, 1211 (1993).
[33] M. V. Volkov and V. N. Ostrovsky, J. Phys. B **37**, 4069 (2004).
[34] B. E. Dobrescu and N. A. Sinitsyn, J. Phys. B **39**, 1253 (2006).
[35] K. Saito and Y. Kayanuma, Phys. Rev. B **70**, 201304(R) (2004).
[36] V. N. Ostrovsky, M. V. Volkov, J. P. Hansen, and S. Selsto, Phys. Rev. B **75**, 014441 (2007).
[37] T. Aoki, T. Kawai, and Y. Takei, J. Phys. A **35**, 2401 (2002).
[38] R. B. Dingle, *Asymptotic Expansions: Their Derivation and Interpretation* (Academic, New York, 1973).
[39] J. Écalle, *Les Fonctions Resergentes* (Publ. Math., Universite de Paris-Sud, 1981), Vol. 3.
[40] A. Voros, Ann. Inst. Henri Poincare A **39**, 211 (1983).
[41] H. J. Silverstone, Phys. Rev. Lett. **55**, 2523 (1985).
[42] F. Pham, Algebraic Anal. **2**, 699 (1988).
[43] E. Delabaere, H. Dillinger, and F. Pham, Ann. Inst. Fourier **43**, 163 (1993); J. Math. Phys. **37**, 6126 (1997).
[44] T. Kawai and Y. Takei, *Algebraic Analysis of Singular Perturbation Theory* (Translations of Mathematical Monographs, AMS, Providence, RI, 2006).
[45] H. L. Berk, W. M. Nevins, and K. V. Roberts, J. Math. Phys. **23**, 988 (1982).
[46] T. Aoki, T. Kawai, and Y. Takei, in *Methodes Resurgentes, Analyse Algebrique des Perturbations Singulieres*, 69th ed. (L. Boutet de Monvel, 1994).
[47] T. Aoki, T. Kawai, and Y. Takei, Asian J. Math. **2**, 625 (1998).
[48] T. Aoki, T. Kawai, T. Koike, S. Sasaki, A. Shudo, and Y. Takei, RIMS Kokyuroku **1424**, 53 (2005).
[49] T. Aoki, N. Honda, T. Kawai, T. Koike, S. Sasaki, A. Shudo, and Y. Takei, *Algebraic Analysis of Differential Equations from Differential Equations from Microlocal Analysis to Exponential Asymptotics Festschrift in Honor of Takahiro Kawai* (Springer, New York, 2007).
[50] T. Aoki, T. Kawai, S. Sasaki, A. Shudo, and Y. Takei, J. Phys. A **38**, 3317 (2005).
[51] N. Honda, T. Kawai, and Y. Takei, *Virtual Turning Points, Springer Briefs in Mathematical Physics* (Springer, New York, 2015).
[52] N. Honda, RIMS Kokyuroku Bessatsu B **10**, 63 (2008).
[53] M. Sato, T. Kawai, and M. Kashiwara, Lect. Notes Math. **287**, 265 (1973).
[54] T. Aoki, T. Koike, and Y. Takei, *Microlocal Analysis and Complex Fourier Analysis* (World Scientific, Singapore, 2002).
[55] A. Shudo and K. S. Ikeda, Nonlinearity **21**, 1831 (2008).
[56] A. Shudo and K. S. Ikeda, Nonlinearity **29**, 375 (2016).
[57] S. Sasaki, RIMS preprint (2015), No.1818.
[58] S. Sasaki, Adv. Math. **301**, 711 (2016).
[59] A. Shudo, RIMS Kokyuroku, 1516, **9** (2005).
[60] J. Heading, *An Introduction to Phase-Integral Methods* (Dover, New York, 2013).
[61] Y. Takei, *Toward the Exact WKB Analysis of Differential Equations, Linear or Non-Linear* (Kyoto University Press, Kyoto, 2000), pp. 271–296.